Plant A20/AN1 proteins coordinate different immune responses including RNAi pathway for antiviral immunity

Li Chang[a,b,c], Ho-Hsiung Chang[b], Yi-Shu Chiu[b], Jui-Che Chang[b], Duen-Wei Hsu[d], Yuh Tzean[b], An-Po Cheng [b], Hsiang-Chia Lu[e], and Hsin-Hung Yeh[b,e#]

[a]Molecular and Biological Agricultural Sciences Program, Taiwan International Graduate Program, National Chung-Hsing University, Academia Sinica, Taiwan

[b]Agricultural Biotechnology Research Center, Academia Sinica, Taipei, Taiwan

[c]Graduate Institute of Biotechnology, National Chung-Hsng University, Taichung, Taiwan

[d]Department of Biotechnology, National Kaohsiung Normal University, Kaohsiung, Taiwan.

[e]Department of Plant Pathology and Microbiology, National Taiwan University, Taipei, Taiwan.

Running Heads: Plant SAPs coordinate RNAi-mediated antiviral immunity

#Address correspondence to Hsin-Hung Yeh, hyeh@sinica.edu.tw

ABSTRACT

Salicylic acid (SA)-mediated immunity plays important roles in combating virus in plants. Two plant stress associated protein (SAPs) containing dual A20/AN1 zinc-finger domain were found to play important roles in SA-mediated immunity; however, detailed mechanisms remain elusive. In this study, another orchid homolog gene of *Pha13*, *Pha21*, was analyzed. Pha21 confers antiviral immunity in both transgenic orchid and *Arabidopsis* overexpressing Pha21. Expression of *Pha21* is early-induced by SA treatment, and is involved in the expression of the orchid homolog of the master regulator *NPR1*. Pha21 but not Pha13 is involved in the expression of key RNAi-related genes, *Dicer-like nuclease 4* (*DCL4*) and *Argonaut 1* (*AGO1*) in orchids. The involvement of SAPs in expression of orchid *DCL4* and *AGO1* is not limited to orchid, as AtSAP5 also plays essential role in the expression of *Arabidopsis DCL4* and *AGO1*. However, unlike Pha13 and AtSAP5, Pha21 does not play positive role in the expression of orchid homolog gene of *RNA-dependent RNA polymerase 1* (*RdR1*), an important gene in RNAi pathway. Pha21 can be found localized in the nucleus, and confers self-E3 ligase and ubiquitin binding activities. Functional domain analysis revealed that both A20 and AN1 domains of Pha21 are required for decreasing virus accumulation, and the AN1 domain plays a more important role in the expression of orchid *DCL4*. Collectively, our data suggests SA regulated SAPs play important roles in antiviral immunity and is involved in delicate regulation of key genes in RNAi-mediated pathway.

IMPORTANCE

Salicylic acid (SA)-mediated antiviral immunity plays an important role to protect plants from virus infection; however, the detailed mechanisms remain elusive. We previously demonstrated that two plant A20/AN1 proteins, orchid Pha13 and *Arabidopsis* AtSAP5, function similarly and serve as an important hub to regulate SA-mediated antiviral immunity. In this study, we identified another orchid A20/AN1 protein, Pha21, which is involved in SA-mediated antiviral immunity. In contrast to Pha13 and AtSAP5, Pha21 plays minor negative roles in the expression of *PhaRdR1* (orchid homolog of *RNA-dependent RNA polymerase 1*). However, Pha21 and AtSAP5, but not Pha13, are involved in the expression of important players in RNAi pathway, *Dicer-like nuclease 4* (*DCL4*) and *Argonaut 1* (*AGO1*), in orchid and *Arabidopsis*. Our data demonstrates that plant A20/AN1 proteins are conserved players in SA-mediated antiviral resistance among plants, and provide links between the A20/AN1 proteins and the RNAi pathway.

INTRODUCTION

The plant hormone salicylic acid (SA) is important to trigger plant immunity especially against biotrophic pathogens such as viruses (1-4). In facing pathogen invasion, plants recognize conserved microbe-associated molecular patterns (MAMPs) by pattern-recognition receptors and trigger pathogen (or pattern)-triggered immunity (PTI) as the first line of defense (5, 6). Although PTI provides protection from invasion by most pathogens, some have evolved, and can utilize different effectors to suppress PTI for successful infection (7). Plants have evolved resistance (R) proteins capable of detecting these effectors to trigger effecter-triggered immunity (ETI) for a second line

of plant defense (7). ETI is generally associated with programmed cell death leading to the formation of necrotic lesions, which is also known as hypersensitive response (HR) to prevent the further spreading of pathogen infection (1).

Current evidence suggests that the PTI is important to limit virus infection (8-10), and the viral double strand RNA (dsRNA) has been shown to serve as a conserved MAMP (10). In addition, ETI also plays an important role in combating virus infection in plants. For example, the N gene from *Nicotiana glutinosa* serves as an R protein to specifically recognize the effector from *Tobacco mosaic virus* (TMV) and trigger the ETI (11-14). SA plays important roles in triggering PTI and ETI (15). In addition, the TMV-infected tobacco plant showing local necrotic lesions was found to become more resistant against secondary virus infection in the distal leaves (16, 17). This systemic immune response is known as systemic acquired resistance, which is a common plant immune response and plays an important role in protecting plants from pathogen infection (4).

In addition, RNA silencing or RNA interference (RNAi) has also been demonstrated to play an important role in combating virus infection (18, 19). RNAi is activated through the appearance of the viral dsRNA upon virus infection. The dsRNA can be cleaved to short small-interfering dsRNA (siRNA) of 21–24 nucleotides (nt) in size by the Dicer-like (DCL) nuclease (20). DCL2 and DCL4 in *Arabidopsis* play an important role in generating the virus-derived siRNA (vsiRNA) (19, 21, 22). The vsiRNA is further unwound and one strand (guide-strand) is incorporated into the RNA-induced silencing complex (RISC) (19). This complex targets viral RNA with a sequence that is complementary to the guide-strand and degrades the target RNA by

91 the catalytic component of the RISC, Argonaut (AGO) nucleases (19, 20, 23, 24).
92 Among the *Arabidopsis* AGOs, AGO1 plays an important role in the antiviral immunity
93 against RNA viruses. (24). More vsiRNA can be further generated *de novo* through the
94 cellular RNA-dependent RNA polymerases (RDRs) to trigger the secondary RNA
95 silencing against viruses (25-27). SA also plays important roles in the RNAi-pathway
96 as SA treatment can induce genes involved in the RNAi pathway including *RDRs* in
97 *Arabidopsis*, *Nicotiana tabacum and* Tomato , and *DCLs* and *AGOs* in Tomato (28-32).
98 SA induces the fluctuation of redox and serves as a signal to activate sets of
99 defense genes (33, 34). The SA-induced redox change can modify the NPR1
100 (nonexpressor of pathogenesis-related protein 1) from the multimeric protein complex
101 to a monomer via the oxidoreductases, Thioredoxin-3 and Thioredoxin-5 (35, 36). The
102 NPR1 monomer moves into the nucleus and activates multiple defense-related genes
103 including the *PR* (*pathogenesis-related*) gene in the SA-signaling pathway (37-39). In
104 addition to the NPR1-dependent immune pathway, some data also suggest that the
105 existence of a NPR1-independent pathway contributes to the virus resistance (40, 41).
106 Despite the importance of the SA governed immune pathway in antiviral immunity, the
107 regulation of this pathway remains largely elusive.
108 Proteins containing zinc-finger A20 and/or AN1 domains play an important role
109 in plant response against various abiotic stresses, and are known as stress associated
110 protein (SAPs). SAPs are conserved among different organisms (42, 43). Different
111 numbers of SAP homologs (range from 1 to 19) have been identified in organisms
112 including protists, fungi, animals, plants, and humans (42, 43). Compared to animals,
113 more of these proteins are found in plants. So far, 18, 14 and 14 SAPs have been

identified in rice, *Arabidopsis*, and *Phalaenopsis* orchid, respectively (42, 44). Biochemical studies of proteins containing A20 and/or AN1 domains revealed that the A20 domain confers E3 ligase and ubiquitin binding activity (43-49). The A20 domain of human A20, Rabex-5 (guanine nucleotide exchange factor), *Arabidopsis* AtSAP5 and orchid Pha13 have been reported to exhibit E3 ligase activity (44, 45, 49, 50). In addition, it has been shown that the A20 domain can also bind to various ubiquitin chains (44, 46-48). In contrast to the A20 domain, the biochemical function of the AN1 domain is not fully understood.

Our recent study indicates that plant SAPs play a pivotal role in SA governed antiviral immunity (44). Orchid *Pha13* and *Arabidopsis AtSAP5* are induced by SA treatment at the early stage, and are involved in expression of orchid or *Arabidopsis NPR1* and *NPR1*-independent immune responsive genes including the induction of plant *RdR1*. In addition to Pha13, our previous virus-induced gene silencing (VIGS) assay also allowed us to identify the involvement of orchid *PhaTF21* (designated here as *Pha21*) in SA–regulated immune response genes (51). Pha13 and Pha21 share 69.5% amino sequence identity, and are most closely related among the orchid SAPs (44). Whether Pha21 and Pha13 work in a cooperative manner in plant antiviral immunity remains to be explored.

Here, we performed a detailed study of Pha21, and compared its biochemical and physiological function to Pha13. Pha21 and Pha13 share similar biochemical properties including E3-ligase and ubiquitin binding activities. Our results also indicate that similar to *Pha13*, *Pha21* is early-induced by SA, involved in the expression of the *PhaNPR1* and *PhaNPR1*-independent genes, and plays an important role in antiviral

immunity. Importantly, our studies show that Pha21 is involved in expression of orchid *DCL4* and *AGO1*. Together with our previous data, these studies suggest that Pha13 and Pha21 coordinate the expression of genes important in the RNAi pathway including orchid *RdR1*, *DCL4* and *AGO1*. In addition, our previous data and data presented in this study also showed that *Arabidopsis* AtSAP5 is involved in expression of *RdR1*, *DCL4* and *AGO1*. Collectively, our data indicates that plant A20/AN1 proteins involved antiviral immunity are conserved among plants, and the antiviral immunity is partly through the RNAi pathway. Our findings suggest that A20/AN1 proteins may serve as a link between SA and the RNAi pathway at the early stage of SA induced-antiviral immunity.

RESULTS

Sequence and expression pattern analysis of Pha21

Previously, we reported that Pha21 (Orchidstra 2.0 database, http://orchidstra2.abrc.sinica.edu.tw, accession number PATC144963) is involved in the SA induced immune pathway in *P. aphrodite* (52). Pha21 contains dual zinc-finger domains, A20 and AN1, in the N-terminal and C-terminal, respectively (Fig. 1A-C), and belongs to the stress associated protein (SAP) family (43). Among the SAPs of *P. aphrodite*, Pha21 is most related to our previously reported Pha13 and shared 69.5% amino acid sequence identity (44). The A20 and AN1 zinc finger domains of Pha21 also shared high amino acid sequence identity among SAPs from different species including AtSAP5 from *Arabidopsis,* and OsSAP3 and OsSAP5 from *Oryza sativa* (Fig. 1B). (44). Unlike Pha13, no nuclear localization signal was identified in Pha21 (Fig. 1A).

160 The expression of *Pha21* was analyzed in different tissues of *P. aphrodite* orchid
161 including root, leaf, septal, petal, lip, and column. The results revealed that *Pha21*
162 expression was higher in the column, root and leaf (Fig. 1D). In addition, we also
163 analyzed the absolute expression of *Pha21* and *Pha13* in the leaves of *P. aphrodite* by
164 use of droplet digital PCR. The results indicated that *Pha21* RNA expression is about
165 15 times lower than *Pha13* in leaves of *P. aphrodite* (Fig. 1E)

166 **Pha21 is involved in the expression of SA responsive genes, *PhaNPR1* and *PhaPR1***

167 To further analyze the role of *Pha21* in the SA-induced immune pathway, we
168 transiently expressed two hairpin RNA (will generate 21 nt siRNA) of Pha21
169 (35S::hpPha21-1 and 35S::hpPha21-2) separately to knockdown Pha21 by
170 agroinfiltration in *P. aphrodite* carrying hairpin RNA expression construct, phpPha21-
171 1 and phpPha21-2 (Fig. 2A). Samples collected from the infiltrated site of orchid leaves
172 were used to detect the RNA level of Pha21, PhaNPR1, and PhaPR1 by quantitative
173 RT-PCR (qRT-PCR). As shown in Fig. 2A, the expression of *PhaNPR1* and *PhaPR1*
174 was decreased in both Pha21-silenced plants. In addition to transient knockdown of
175 Pha21, we also transiently overexpressed Pha21 (35S::FLAG-Pha21) through
176 agroinfiltration in the leaves of *P. aphrodite.* However, transient overexpression of
177 Pha21 in leaves did not significantly affect the RNA level of PhaNPR1 and PhaPR1
178 (Fig. 2B).

179 In addition, we also transiently silenced PhaNPR1 (phpPhaNPR1) in *P. aphrodite*
180 to analyze the expression of *Pha21*. The results showed that the silenced PhaNPR1
181 showed decreased expression of *PhaPR1*; however, no obvious effect was observed on

182 the expression of *Pha21* (Fig. 2C). These results suggest that Pha21 is involved in the
183 expression of *PhaNPR1*, but not vice versa.

184 **_Pha21_ is induced by SA, jasmonic acid and ethylene**

185 We also tested whether *Pha21* was induced by defense-related plant hormones
186 including SA, jasmonic acid (JA) and ethylene (ET). Orchid plants were treated with
187 SA, JA and ET and samples were collected after treatment at different time points (up
188 to 72 h) for analysis of the expression of *Pha21* and the marker genes of each plant
189 hormone by qRT-PCR. The induction of *Pha21* by SA was observed at 1 h post-
190 treatment (Fig. 2D). In addition, *Pha21* was also induced by JA and ET at 72 h and 12
191 h, respectively (Fig. 2E and F). Our results showed that *Pha21* can respond to multiple
192 defense-related plant hormones, and SA induced *Pha21* expression at the very early
193 stage.

194 **Pha21 plays a positive role in virus resistance**

195 To analyze whether Pha21 plays a role in virus resistance, we first analyzed the
196 expression of *Pha21* in response to virus infection. We detected the RNA level of Pha21
197 in mock- or CymMV-inoculated *P. aphrodite* using qRT-PCR, and the results showed
198 that the RNA of Pha21 is induced by CymMV infection (Fig. 3A). Furthermore, we
199 transiently silenced or overexpressed Pha21 in CymMV-infected *P. aphrodite* to assay
200 the effect on virus accumulation. Transient knockdown of Pha21 had no significant
201 effect on CymMV accumulation (Fig. 3B); whereas transient overexpression of Pha21
202 decreased CymMV accumulation (Fig. 3C). In addition, we also generated transgenic
203 *P. equestris* overexpressing Pha21 (35S::FLAG-Pha21). The expression of *Pha21* is
204 higher in the two individual asexually propagated progeny derived from two T0 lines

of transgenic *P. equestris* (Pha21#8 and Pha21#9) as compared to the non-transgenic lines (WT) (Fig. 3D). We further inoculated CymMV into individual progenies derived from two transgenic lines, and the result showed that the accumulation level of CymMV is decreased to 21% and 34% in the two transgenic lines (Pha21#8 and Pha21#9) as compared to the non-transgenic lines (WT) (Fig. 3D). Our data suggest that Pha21 plays a positive role in virus resistance.

Transgenic *Arabidopsis* overexpressing Pha21 enhances antiviral resistance.

To understand whether Pha21-mediated antiviral immunity is conserved in plants, we generated the transgenic *Arabidopsis* (Col-0) overexpressing Pha21 (35S::FLAG-Pha21). Homozygous T3 plants derived from 3 T1 transgenic lines, At-Pha21#4, #5 and #6, were selected for further antiviral assay. The expression level of *Pha21* was confirmed by qRT-PCR on the homozygote progenies (Fig. 4A).

We mechanically inoculated *Cucumber mosaic virus* (CMV) to wild-type (WT) and Pha21 overexpressing *Arabidopsis* (At-Pha21#4, #5 and #6). Fourteen days post-inoculation, the accumulation of CMV in WT and Pha21 overexpressing *Arabidopsis* were detected by qRT-PCR. The results showed that Pha21 overexpressing *Arabidopsis* decreased the accumulation of CMV (Fig. 4A) compared to the WT, and severe disease symptoms were observed on the WT but not in the Pha21 overexpressing *Arabidopsis* (Fig. 4B).

Subcellular localization of Pha21

To better understand the role of Pha21 within cells, we first analyzed the subcellular localization of Pha21. We fused green fluorescent protein (GFP) in the N- or C-terminal of Pha21 driven by 35S promoter (pG-Pha21 and pPha21-G). The GFP-

fused Pha21 was further transfected into protoplasts isolated from *P. aphrodite.* Twenty-four hours post-transfection, the localization of Pha21 was observed by using a confocal microscope. The results indicated that the C-terminal GFP fusion protein (Pha21-G) was observed in the nucleus in about 50% of cells; whereas the N-terminal GFP fusion protein (Pha21-G) showed a similar result to our GFP control vector, which had no nucleus-specific GFP (Fig. 5A). Our data suggested that Pha21 can move into the nucleus even without the predicated NLS signal.

Pha21 and Pha13 does not confer transcriptional activation ability in yeast two-hybrid assay

Since both Pha21 and Pha13 have the ability to move into the nucleus (44), we tried to understand whether Pha21 and Pha13 function as transcription factors. Therefore, we analyzed its transcriptional activation ability through yeast two-hybrid (Y2H) assay. We fused Pha21 and Pha13 to the Gal4 DNA binding domain to generate pGBKT7-Pha21 and pGBKT7-Pha13. We transformed the pGBKT7-Pha21 or pGBKT7-Pha13 in the yeast strain AH109 without any Gal4 transcriptional activation domain (AD) and further analyzed the transcriptional activation ability through the analysis of the activation of reporter genes in yeast. As shown in Fig. 5B, yeast with pGBKT7-Pha21 or pGBKT7-Pha13 cannot grow on the -Trp/Aureobasidin and -Trp/-Ade/-His medium, and the colonies did not turn blue on X-α-Gal containing medium.

Pha21 exhibits E3 ligase activity in which the A20 domain plays a major role

Several A20 and/or AN1 domain containing proteins confer E3 ligase activity (44-46, 53). To determine whether Pha21 functions as an E3 ligase, *in vitro* self-ubiquitination E3 ligase activity assay was performed using FLAG-Ubiquitin (FLAG-

Ub), human E1 (hE1), human E2 (UBCH2, hE2), and purified His-tagged Pha21 (Pha21-His). The poly-ubiquitinated Pha21 can be detected in the presence of FLAG-Ub, hE1, and hE2 using anti-FLAG antibody to detect FLAG-Ubiquitin. The results revealed that Pha21 confers E3 ligase activity (Fig. 6A).

Furthermore, we also analyzed the self-ubiquitination E3 ligase activity of the A20 and/or AN1 domain of Pha21. We substituted the conserved cysteine and histidine to glycine on the A20 and/or AN1 domains of Pha21-His (Fig 1B and C) to generate A20 domain mutant (Pha21-A20m), AN1 domain mutant (Pha21-AN1m), and the double mutant (Pha21-A20mAN1m) for E3 ligase activity analysis. As shown in Fig 6A, the major E3 ligase activity was conferred by the A20 domain. A20 domain mutant and double mutant of Pha21 showed lower self-ubiquitination E3 ligase activity than wild-type Pha21 and Pha21-AN1 mutant (Fig. 6A).

A20 domain of Pha21 confers ubiquitin binding ability

A20 and/or AN1 proteins have also been shown to confer ubiquitin binding ability in animals and plants (44, 46, 47, 54, 55). To analyze whether Pha21 has ubiquitin binding ability, Y2H assay was performed to verify the interaction using Pha21 as bait and ubiquitin as prey. As shown in Fig 6B, Pha21 had a positive interaction with ubiquitin, suggesting that Pha21 conferred ubiquitin binding ability. In addition, to identify the ubiquitin binding domain of Pha21, a series of deletion mutants of Pha21 were generated, followed by Y2H assay. The result revealed that only truncated Pha21 fragments containing A20 domain ($Pha21^{1-136}$, $Pha21^{1-101}$, $Pha21^{1-40}$, $Pha21^{16-158}$, $Pha21^{16-136}$, $Pha21^{16-101}$, $Pha21^{16-40}$) showed a positive interaction with ubiquitin,

suggesting that the A20 domain of Pha21 is responsible for the ubiquitin binding ability (Fig. 6B).

Interaction analysis between orchid SAPs

The A20/AN1 proteins may confer self-interaction and also interact with each other (56). Therefore, we also analyzed whether Pha21 and Pha13 confer self-interaction and also interact with each other. The Y2H assay was performed to verify the interaction between Pha21 and Pha13. Our Y2H results suggested that Pha21 and Pha13 did not interact with each other and no self-interaction of Pha21 or Pha13 was observed (Fig. 7).

Pha21 is involved in the expression of SA-induced PhaNPR1-dependent and -independent genes.

To further understand how Pha21 is involved in the antiviral immunity, we performed transient silencing (35S::hpPha21-2) and overexpression assay (35S::FLAG-Pha21) of Pha21 in *P. aphrodite*, and analyzed the expression of the previously identified PhaNPR1-dependent and -independent antiviral genes, *Phalaenopsis* homolog of *RNA dependent RNA polymerase 1* (*PhaRdR1)* and *Glutaredoxin C9 (PhaGRXC9)*, respectively (44). Our results indicated that transient silencing of Pha21 RNA increased the expression of *PhaRdR1*, while *PhaGRXC9* remained unchanged (Fig. 8A). Transient overexpression of Pha21 RNA decreased the expression of *PhaGRXC9*, but *PhaRdR1* remain unchanged (Fig. 8B). Our data suggest that Pha21 affects the expression of *PhaRdR1* and *PhaGRXC9*.

Pha21 is involved in the expression of *PhaDCL4* and *PhaAGO1*

295 Because the RNAi pathway plays an important role in antiviral immunity (18, 19),
296 we analyzed whether Pha21 is involved in the expression of core RNAi-related genes
297 including the *Phalaenopsis* homolog genes of *RdR2* (*PhaRdR2*, PATC124544), *RdR6*
298 (*PhaRdR6*, PATC131836), *DCL2* (*PhaDCL2*, PATC143544), *DCL4* (*PhaDCL4*,
299 PATC150652), *AGO1* (*PhaAGO1*, PATC157237), and *AGO10* (*PhaAGO10*,
300 PATC093469). Transient overexpression and silencing assay of Pha21 was performed
301 in *P. aphrodite*. Overexpression of Pha21 increased the RNA expression of *PhaDCL4*
302 and *PhaAGO1* (Fig. 9A); whereas transient silencing of Pha21 had no significant effect
303 on the RNA expression of RNAi-related genes (Fig. 9B).

304 For comparison, we also analyzed the effect of Pha13 on the RNAi-related genes.
305 The results showed that transient overexpression of Pha13 has no significant effect on
306 the expression of *PhaRdR2*, *PhaRdR6*, *PhaDCL2*, *PhaDCL4*, *PhaAGO1*, *and*
307 *PhaAGO10* (Fig. 9C). Our results suggested that Pha21 is involved in the expression
308 of *PhaDCL4* and *PhaAGO1*.

309 To see whether orchid DCL4 (PhaDCL4) and AGO1 (PhaAGO1) also play a role
310 in the antiviral immunity, we transiently silenced PhaDCL4 and PhaAGO1 through
311 delivering the hairpin RNA into *P. aphrodite* by agroinfiltration carrying hairpin RNA
312 expression constructs, phpPhaDCL4 and phpPhaAGO1. Our results showed that
313 transient silencing of PhaDCL4 and PhaAGO1 increased the accumulation of CymMV
314 (Fig. 9D and E).

315 **The *Arabidopsis* homolog gene of *Pha21*, *AtSAP5*, is involved in the expression**
316 **of *DCL4* and *AGO1*.**

317 Our previous phylogenic analysis revealed that both Pha21 and Pha13 are closely
318 related to *Arabidopsis* AtSAP5 (accession number: AT3G12630) (44). Therefore, we
319 also analyzed whether AtSAP5 is involved in the expression of *DCL4* and *AGO1*. We
320 detected the expression of *DCL4* and *AGO1* in our previously generated transgenic
321 *Arabidopsis* overexpressing AtSAP5 (AtSAP5-oe-4 and 11) and RNAi lines of AtSAP5
322 (AtSAP5-RNAi-3 and 7) by qRT-PCR (44). The expression level of *AtSAP5* was
323 confirmed by qRT-PCR (Fig. 10A). Our results showed that slightly increased
324 expression of *DCL4* and *AGO1* were observed in overexpression transgenic lines,
325 AtSAP5-oe-11 and decreased expression of *DCL4* and *AGO1* were observed in the
326 RNAi lines, AtSAP5-RNAi-3 and AtSAP5-RNAi-7 (Fig. 10B and C). Our results
327 suggest that AtSAP5 is important in the expression of *DCL4* and *AGO1*.

328 **A20 and AN1 domain of Pha21 play different roles in the expression of *PhaDCL4,***
329 ***PhaAGO1, PhaGRXC9* and virus resistance.**

330 Our previous results indicated that Pha21 is involved in the expression of
331 *PhaDCL4*, *PhaAGO1*, and *PhaGRXC9* and virus accumulation (Figs 3C, 3D, 8B, and
332 9A). We further analyzed the roles of the A20 and/or AN1 domains of Pha21 in the
333 expression of *PhaDCL4*, *PhaAGO1*, *PhaGRXC9* and virus accumulation by
334 overexpression of Pha21 and Pha21 with mutation in the A20 and/or AN1 domain.
335 Therefore, we generated Pha21 with A20 domain mutant (Pha21A20m), AN1 domain
336 mutant (Pha21AN1m), and the double mutant (Pha21A20mAN1m) through the
337 substitution of the conserved cysteine and histidine to glycine on A20 and/or AN1
338 domain (Fig. 1B and C). We transiently overexpressed wild-type Pha21 or the mutants
339 (A20 and/or AN1 domain mutant) in healthy or CymMV pre-infected *P. aphrodite*, and

then detected *PhaDCL4, PhaAGRO1, PhaGRXC9,* and CymMV. The results indicated that overexpression of Pha21 A20 mutant (Pha21A20m) but not AN1 mutant (Pha21AN1m) or A20/AN1 mutant (Pha21A20mAN1m) increased the expression of *PhaDCL4*, which is similar to the wild-type Pha21 (Fig. 11A). Overexpression of any Pha21 A20 and/or AN1 mutant showed similar results to wild-type Pha21 with respect to increased expression of *PhaAGO1* (Fig. 11A). Although overexpression of wild-type and any Pha21 A20 and/or AN1 mutant resulted in decreased expression of *PhaGRXC9* and CymMV accumulation compared to the vector control, overexpression of wild-type Pha21 showed a greater effect on the expression of *PhaGRXC9* and CymMV accumulation compared to any Pha21 A20 and/or AN1 mutant (Fig. 11A and B). Our data suggest that both the A20 and AN1 domains of Pha21 are required for expression of *PhaGRXC9* and the decrease of CymMV accumulation, and the AN1 domain plays a major role in the expression of *PhaDCL4*. They also suggest that neither domain is required for the expression of *PhaAGO1*.

DISCUSSION

Plant A20/AN1 proteins, Pha13, Pha21 and AtSAP5 share similar biochemical properties and all involved in SA-mediated antiviral immunity

In this report, we performed detailed analysis of a previously identified orchid gene, *Pha21*, involved in SA and RNAi-mediated antiviral immunity. Pha21 shares high protein sequence identity to our previously identified Pha13 (Fig. S7 in Chang et al, 2018), and exhibits similar biochemical properties including self-E3 ligase, ubiquitin binding abilities (Fig. 6) and subcellular localization (Fig. 5A). Similar to Pha13, our

363 data suggests that Pha21 is involved in the SA-signaling pathway downstream of SA
364 and upstream of the expression of *PhaNPR1* (Fig. 2A, C and D). In addition, Pha13 and
365 Pha21 also positively mediate antiviral immunity (44). Transgenic *Arabidopsis*
366 overexpressing Pha21 also enhanced resistance to virus infection (Fig 4) (44). In
367 addition, our previous report and the data presented here indicate that *Arabidopsis*
368 AtSAP5 is also induced by SA at the early stage, and is involved in expression of similar
369 sets of SA mediated immune responsive genes, and positively regulates antiviral
370 immunity (44).

371 **Pha13-mediated expression of *PhaGRXC9* and *PhaRdR1* are dominant during SA**
372 **treatment.**

373 Our previous study indicated that Pha13 and AtSAP5 plays a positive role in the
374 expression of genes involved in the RNAi pathway and SA-governed oxidoreductases,
375 *RdR1* and *GRXC9*, respectively (44). We demonstrated that both PhaRdR1 and
376 PhaGRXC9 play positive roles in antiviral immunity (44). In this study, we found that
377 Pha21 has an opposite role to Pha13 in the expression of *PhaRdR1* and *PhaGRXC9*
378 (Fig. 8). As our data indicates that the RNA level of Pha13 is approximately 15 times
379 higher than Pha21 in leaves of orchids as measured by digital PCR (Fig. 1E), we suggest
380 that the effect of Pha21 on the expression of *PhaRdR1* and *PhaGRXC9* is minor, and
381 Pha13-mediated positive expression of *PhaGRXC9* and *PhaRdR1* are dominant during
382 SA treatment.

383 **Pha21 and AtSAP5 are all involved in expression of key genes in RNAi pathway,**
384 **but regulation of *PhaDCL4* and *PhaAGO1* by Pha21 in orchid is different from**
385 **regulation of *DCL4* and *AGO1* by AtSAP5 in *Arabidopsis***

Our data indicates that similar to *Arabidopsis* DCL4 and AGO1, orchid PhaDCL4 and PhaAGO1 also play a similar positive role in antiviral immunity in orchids as a slight decrease in the RNA of PhaDCL4 or PhaAGO1 (approximately 40% decrease) has a prominent effect on CymMV accumulation (approximately 100% increase) (Fig. 9D and E), (19). Interestingly, our data suggests that Pha21 regulates antiviral immunity partly through the effect on the RNAi pathway, as transient overexpression of Pha21 (1.6-folds) but not Pha13 increased the expression of two *Phalaenopsis* orchid homolog genes of *DCL4* (*PhaDCL4*, 2-fold) and *AGO1* (*PhaAGO1*, 1.6-fold) (Fig. 9A and C).

Although the effect of AtSAP5 on expression of *DCL4* and *AGO1* is not as prominent as Pha21, our data shown here also indicates that AtSAP5 is involved in the expression of *DCL4* and *AGO*1. In both of our silencing lines, AtSAP5-RNAi-3 and -7 showed noticeable effect on the expression of *DCL4* and *AGO1* (Fig. 10), but that only one overexpression line, AtSAP5-oe-11 (expression increased about 7 times over AtSAP5) slightly increased the expression of *DCL4* (40% increase) and *AGO1* (20% increase). This suggests that AtSAP5 is still important for the maintenance of *DCL4* and *AGO1* expression.

Collectively, our data suggests that although Pha13 and Pha21 both participate in SA regulated immunity, they act differently in triggering downstream immune responsive genes.

Pha13 and Pha21 showed no transcriptional activation activity by Y2H assay

Although Pha21 and Pha13 are involved in expression of *PhaGRXC9*, *PhaRdR1*, *PhaDCL4* and *PhaAGO1*, our Y2H analysis showed that Pha21 and Pha13 have no transcriptional activation activity (Fig. 5B).

A20 confers most E3 ligase and ubiquitin binding activity but the AN1 domain also plays important roles in expression of immune responsive genes.

Similar to other analyzed A20/AN1 proteins, our biochemical assay indicated that both Pha21 and Pha13 confer E3 ligase activity and ubiquitin binding ability, and A20 domain of Pha21 and Pha13 is the major domain exhibiting self-E3 ligase and ubiquitin binding activity (Fig. 6) (44). It has been well demonstrated that human A20 proteins (without an AN1 domain) regulate the master immune transcription factor NF-kB through ubiquitin editing activity including E3 ligase and ubiquitin binding ability on different substrates (53). It is likely that Pha21 and Pha13 may function in a similar manner to human A20 indirectly, rather than directly function as transcription factors.

Our previous domain functional analysis revealed that both the A20 and AN1 domains of Pha13 are required for expression of *PhaRdR1*, *PhaGRXC9*, and virus accumulation, and the AN1 domain of Pha13 is involved in the expression of *PhaNPR1* (44). Here we also showed that A20 and AN1 domains of Pha21 are both required for expression of *PhaGRXC9* and CymMV accumulation, and the AN1 domain plays a more important role in the expression of *PhaDCL4* (Fig. 11). This indicates that although A20 confers most E3 ligase and ubiquitin binding activity, the AN1 domain also plays important roles in expression of immune responsive genes. Interestingly, our data suggests that neither domain of Pha21 is required for the expression of *PhaAGO1*, which suggests that protein regions other than A20 and AN1 domain in Pha21 are also involved in the expression of *PhaAGO1* (Fig. 11A).

A20/AN1 proteins serve as important modulators in plant antiviral immunity

Our previous data and the findings presented here indicate that A20/AN1 protein-mediated antiviral immunity is conserved among plants, and A20/AN1 proteins may work alone (AtSAP5) or in a cooperative manner (Pha13 and Pha21) in antiviral immunity to induce the expression of the SA-mediated immune responsive genes, including *NPR1*, NPR1-independent oxidoreductases gene (*GRXC9*), and genes involved in the RNAi pathway *(RdR1*, *AGO1* and *DCL4*) (Fig. 12).

MATERIALS AND METHODS.

Plant materials and growth conditions

Orchid variety, *Phalaenopsis aphrodite var. Formosa*, was purchased from Taiwan Sugar Research Institute (Tainan, Taiwan). All orchid plants we used including *P. aphrodite, P. equestris* and transgenic *P. equestris* (35S::FLAG-Pha21) were first analyzed for the infection with two prevalent orchid viruses, *Odontoglossum ringspot virus* (ORSV) and CymMV, as detected by RT-PCR with primer pairs, ORSV-F/ORSV-R and CymMV-F/CymMV-R (Table 1). Plants free from ORSV and CymMV were maintained in greenhouse conditions with a controlled 12-h photoperiod (200 μmol $m^{-2}s^{-2}$) at 25°C/25°C (day/night). The wild-type (WT) *Arabidopsis* WT (Col-0) and all transgenic *Arabidopsis* were maintained in a greenhouse with a controlled 12-h photoperiod (200 μmol m-2s-2) at 22°C/22°C (day/night) for three to four weeks before analysis. *Cucumber mosaic virus* (CMV) isolate 20 was maintained in the *Arabidopsis* (Col-0) as inoculation source in our study.

Sequence analysis

452 The amino acid sequence of Pha21 was analyzed by the PROSITE database,
453 ExPASy Proteomics Server (http://ca.expasy.org/), and Conserved Domain Database
454 of NCBI database (http://www.ncbi.nlm.nih.gov/).
455
456 **Phytohormone treatment**
457 Sodium salicylate (50 mM) (Sigma, St. Louis, MO, USA), methyl jasmonate (45
458 μM) (Sigma), and aminocyclopropanecarboxylic acid (660 μM) (Sigma) were directly
459 rubbed on leaves of *P. aphrodite* by cotton swab. Leaf samples were collected at 0 h, 1
460 h, 3 h, 6 h, 12 h, 24 h, 48 h and 72 h after treatment.
461
462 **RNA isolation and real-time quantitative RT-PCR (qRT-PCR) detection**
463 Total RNA was extracted using the TOOLSmart RNA Extractor (BIOTOOLS,
464 Taiwan) as described previously (44). The cDNA template for qPCR was synthesized
465 from 500 ng of DNA-free RNA and oligo (dT) using PrimeScript RT Reagent Kit
466 (Perfect Real Time), following the manufacturer's instructions (Takara Bio, Shiga,
467 Japan). qPCR was performed using SYBR Green PCR Master Mix (Applied
468 Biosystems, Foster, CA, USA)) with ABI Prism 7500 sequence detection system
469 (Applied Biosystems). Target gene PCR products were sequenced to validate the
470 correct analysis of gene targets. *PhaUbiquitin 10* or *AtActin* was used as an internal
471 quantification control. Quantification of target gene expression was calculated
472 according to the manufacturer's instructions (Applied Biosystems). The primer pairs
473 used in this study are listed in Table 1.

474

475 **Droplet digital PCR**

476 Total RNA was extracted using the TOOLSmart RNA Extractor (BIOTOOLS,
477 Taiwan) as described previously (44). For droplet digital PCR (ddPCR), DNA-free
478 RNA (1 μg) and oligodT primer were used for cDNA synthesis with PrimeScript RT
479 Reagent Kit (Perfect Real Time) following the manufacturer's instructions (Takara
480 Bio). An amount of 5 μl of 25X dilute cDNA was used as a template for ddPCR reaction
481 (total 20 μl) following the manufacturer's instructions (Bio-Rad, Hercules, CA, USA).
482 The sequence of FAM-labeled Taqman probes and primer pairs of Pha13 and Pha21
483 for ddPCR are listed in Table 1.

484

485 **Construction of transient silencing vector**

486 For construction of transient silencing vector of Pha21, the oligonucleotide pairs
487 Pha21-hpRNA-1-F/Pha21-hpRNA-1-R and Pha21-hpRNA-2-F/Pha21-hpRNA-2-R
488 (Table 1) were used to amplify the hairpin dsDNA fragments. The hairpin dsDNA
489 fragments were cloned into the Gateway entry vector pENTR/D-TOPO (Thermo
490 Fisher-Scientific, Waltham, MA, USA) following the manufacturer's instructions to
491 generate pENTR-Pha21-hpRNA-1 and pENTR-Pha21-hpRNA-2. Then, LR Gateway
492 cloning reaction (Thermo Fisher-Scientific) was conducted to transfer the hairpin RNA
493 fragments from pENTR-Pha21-hpRNA into 35S promoter driven pB7GWIWG2(I) (57)
494 to obtain phpPha21-1 and phpPha21-2. The method for construction of the transient
495 silencing vector of *PhaNPR1, PhaDCL4, and PhaAGO1* (phpPhaNPR1, phpPhaDCL4,
496 and phpPhaAGO1) were similar to that described above, except the oligonucleotide

497 pairs PhaNPR1-hpRNA-F/PhaNPR1-hpRNA-R, PhaDCL4-hpRNA-F/PhaDCL4-
498 hpRNA-R, and PhaAGO1-hpRNA-F/ PhaAGO1-hpRNA-R (Table 1) were used to
499 generate the hairpin dsDNA fragments.
500
501 **Construction of transient overexpression vector of Pha21, Pha21 A20 and/or AN1**
502 **domain mutant.**
503 To construct Pha21 transient overexpression vector, total *P. aphrodite* RNA was
504 used as a template to amplify the N-terminus FLAG-tagged Pha21 by RT-PCR with the
505 primer pairs FLAG-Pha21ORF-F/Pha21ORF-R (Table 1). The amplified fragment was
506 cloned into Gateway entry vector pENTR/D-TOPO (Invitrogen) to generate pENTR-
507 FLAG-Pha21 following the manufacturer's protocol. Subsequently, LR Gateway
508 cloning reaction (Invitrogen) was performed to transfer the FLAG-Pha21 fragment
509 from pENTR-FLAG-Pha21 into the 35S promoter driven pK2GW7 (57), designated
510 pPha21-oe. For generation of A20 and/or AN1 mutant on pPha21-oe (Fig. 1), site-
511 directed mutagenesis was conducted by QuikChange Site-Directed Mutagenesis Kit
512 (Agilent Technologies, Santa Clara, CA, USA) and pPha21-oe was used as a template.
513 For A20 mutant, we substituted the conserved 3rd and 4th cysteine to glycine at A20
514 (C35G and C38G). For AN1 mutant, we substituted the conserved 3rd cysteine and 1st
515 histidine to glycine at AN1 (C113G and H123G). The A20 mutated clones, AN1
516 mutated clones, and the A20 and AN1 mutated clones, were designed as pPha21A20m,
517 pPha21AN1m, and pPha21A20mAN1m, respectively. Primer pairs used for site
518 directed mutagenesis are listed in Table 1.
519 **Transgenic *Phalaenopsis* orchid**

520 For construction of overexpression vector to generate transgenic *Phalaenopsis*
521 orchid, the FLAG-Pha21 fragment was transferred from pENTR-FLAG-Pha21
522 (described above) into 35S promoter driven binary vector, pH2GW7 (57), to obtain
523 pHPha21. pHPha21 was used to generate transgenic *P. equestris* orchid using the
524 method described by Hsing et al. (58).
525
526 **Agroinfiltration**
527 Agroinfiltration was conducted as previously described by (51) with some
528 modification. Briefly, *A. tumefaciens* C58C1 (pTiB6S3ΔT)^{H} competent cells were
529 transformed with pCambia-CymMV, pB7GWIWG2, pK2GW7 and their derivatives
530 using an electroporation system (Bio-Rad Laboratories, Hercules, CA, USA). Then, the
531 *A. tumefaciens* strains were incubated at 28°C until the optical density, OD_{600}, reached
532 0.8–1.0. After centrifugation, cells were resuspended in 20 ml AB-MES medium (17.2
533 mM K_2HPO_4, 8.3 mM NaH_2PO_4, 18.7 mM NH_4Cl, 2 mM KCl, 1.25 mM $MgSO_4$, 100
534 µM $CaCl_2$, 10 µM $FeSO_4$, 50 mM MES, 2% glucose (w/v), pH 5.5) with 200 µm
535 acetosyringone (59), and cultured overnight. The overnight culture was centrifuged
536 (3000 rpm, 10 min, in room temperature), supernatant was removed and the *A.*
537 *tumefaciens* culture was resuspended in 2 ml of infiltration medium containing 50%
538 MS medium (1/2 MS salt supplemented with 0.5% sucrose (w/v), pH 5.5), 50% AB-
539 MES and 200 µm acetosyringone (59). The infiltration medium containing the
540 transformed *A. tumefaciens* was applied for infiltration.
541

542 ***Cymbidium mosaic virus*** **(CymMV) and** ***Cucumber mosaic virus*** **(CMV) inoculation**
543 **and accumulation assay**

544 To assay the effect of Pha21, PhaDCL4, or PhaAGO1 in CymMV accumulation,
545 we first inoculated CymMV in *P. aphrodite* through the infiltration of *A. tumefaciens*
546 carrying pCambia-CymMV (described above) in the leaf tip of *P. aphrodite*. The
547 CymMV-infected *P. aphrodite* was maintained at least 14 days before further analysis.
548 To assay the effect of transient silencing (Pha21, PhaDCL4, or PhaAGO1) or transient
549 overexpression (Pha21, or the derived mutants), *A. tumefaciens* carrying the control
550 vector pB7GWIWG2 (for silencing), pK2GW7 (for overexpression), silencing vectors
551 or overexpression vectors (described above) were infiltrated into the leaves. After
552 agroinfiltration, a pair of disks (6 mm diameter) were immediately (defined as 0 dpi)
553 collected from both the control and assay vector infiltrated regions. After 5 dpi, another
554 pair of disks were collected from the same infiltrated region. Total RNA extracted from
555 the samples was used as a template to analyze the accumulation of CymMV by use of
556 qRT-PCR. The fold change of CymMV accumulation at 0 dpi to 5 dpi was calculated
557 for relative quantification.

558 For inoculation with CMV, CMV-infected *Arabidopsis* leaves were ground with
559 0.01 M potassium phosphate buffer by pestle and mortar for use as the inoculation
560 source. Four-week-old *Arabidopsis* leaves were inoculated mechanically (pre-dusted
561 with 300-mesh Carborundum) with the CMV inoculation source. After 14 dpi, the
562 disease symptoms were observed, and three disks from three different distal leaves were
563 collected for CMV accumulation analysis by use of qRT-PCR. Primers used for CMV
564 detection are listed in Table 1.

565

566 **Preparation and transfection of protoplasts**

567 For construction of vectors used for subcellular localization analysis, the primer
568 pairs, Pha21-ORF-F/Pha21-ORF-R and Pha21-ORF-F/Pha21-ORF-non-stop-R (Table
569 1) were used to amplify 2 sets of Pha21 ORF (with or without a stop codon). The
570 amplified fragment was cloned into Gateway entry vector pENTR/D-TOPO (Invitrogen)
571 to generate pENTR-Pha21 and pENTR-Pha21-non-stop following the manufacturer's
572 protocol. Subsequently, LR Gateway cloning reaction (Invitrogen) was performed to
573 transfer ORF fragment of *Pha21* from pENTR-Pha21 into p2FGW7 driven by 35S
574 promoter (57) to obtain N-terminal GFP fused clones (pG-Pha21). To obtain C-terminal
575 GFP-fused clones (pPha21-G), we transferred and pENTR-Pha21-non-stop into
576 p2GWF7.

577 Protoplast isolation and transfection were as described by Lu et al. (51).
578 Transformed protoplasts were detected for florescence signals by confocal microscopy
579 (Zeiss LSM 780, plus ELYRA S.1) with excitation at 488 nm and emission at 500 to
580 587 nm for GFP, and excitation at 543 nm and emission at 600 to 630 nm for mCherry.

581

582 **Transcriptional activation ability assay**

583 The Pha13 and Pha21 ORF was amplified by PCR with gene specific primer pairs,
584 NdeI-Pha13-F/EcoR1-Pha13-R and NdeI-Pha21-F/BamH1-Pha21-R, respectively
585 (Table 1). The amplified ORF fragment was then cloned into the pGBKT7 vector
586 (Takara Bio) to generate the pGBKT7-Pha13 and pGBKT7-Pha21 constructs, which
587 fused to Gal4 BD sequence. These constructs were individually transformed into

AH109 yeast strain (Takara Bio) and the self-activation ability was analyzed. The transformation and selection procedure was performed following the Yeast Protocols HandBook (Takara Bio). Transformants were selected on SD/-Trp (tryptophan) medium. The expression of reporter genes in yeast were tested on different selection media; SD/-Trp/Aureobasidin was used to test for activation of the AUR1-C (inositol phosphoryl ceramide synthase) reporter against Aureobasidin A, SD/-Trp/X-α-Gal medium was used to test for activation of α-galactosidase, and SD/-Trp/-Ade/-His medium was used to test for induction of the ADE2 and HIS3 reporters. The yeast containing Gal4 DNA-BD fused with murine p53 (pGBKT7-53) and the Gal4 AD fused with SV40 large T-antigen (pGADT7-T) from the Matchmaker Gold Yeast Two-Hybrid System kit (Takara Bio) were used as positive control. The yeast containing Gal4 DNA-BD fused with lamin (pGBKT7-Lam) and the pGADT7-T from the Matchmaker Gold Yeast Two-Hybrid System kit (Takara Bio) were used as a negative control.

Construction, expression, and purification of recombinant proteins

Full-length Pha21, or Pha21 A20 and/or AN1 domain mutant fragments were amplified by PCR with primer pairs NdeI-Pha21-F/NotI-Pha21-R (Table 1) using pPha21-oe, pPha21A20m, pPha21AN1m, and pPha21A20mAN1m as templates. The amplified fragments were cloned into the pET24b expression vector (Merck, Darmstadt, Germany) to produce fused C-terminal histidine tag (His-tag) expression plasmids, pETPha21, pETPha21A20m, pETPha21AN1m and pETPha21A20mAN1m. The constructed plasmids were transformed into *Escherichia coli* strain BL21 (DE3) for

611 protein expression. Bacteria were cultured at 37°C to an OD600 of 0.5, then transferred
612 to 25°C, for 1.5 h. Then, isopropylthio-β-galactoside (IPTG; Sigma) was added to a
613 final concentration of 1 mM for protein induction. His-tagged recombinant protein was
614 purified by TALON Superflow (GE Healthcare Life Sciences, Pittsburgh, PA, USA)
615 according to the manufacturer's description. His-tagged recombinant protein was
616 eluded with 250 mM imidazole (Sigma).
617
618 **E3 ubiquitin ligase activity assay**
619 *In vitro* ubiquitination assays were performed as described by (45) with
620 modification. An amount of 3 μg purified His-tagged recombinant proteins (*Pha21* or
621 derived mutants) was used for each ubiquitination reaction. Reactions were incubated
622 at 30°C for 3 hours and analyzed by SDS-PAGE followed by immunoblot analysis.
623 Blots were probed using anti-FLAG antibodies (Sigma) followed by HRP conjugated
624 goat anti-mouse antibodies (GE Healthcare Life Sciences).
625
626 **Yeast two-hybrid assay**
627 For the ubiquitin binding ability assay, the pGBKT7-Pha21 (described above)
628 was used as a bait vector. To map the region of Pha21 for ubiquitin binding, a deletion
629 mutant of Pha21 was generated by PCR amplification with the primer pairs described
630 in Table 1. The PCR-amplified fragment was individually cloned to pGBKT7 and used
631 as a bait vector (Fig. 6B). Full length of orchid ubiquitin was amplified by RT-PCR
632 with the primer pair, NdeI-PhaUBQ-F/BamHI-PhaUBQ-R, and cloned into pGADT7
633 vector (Takara Bio) to generate pGADT7-UBQ as a prey vector. pGBKT7-Pha21 and

pGADT7-UBQ was co-transformed into AH109 yeast strain for yeast two-hybrid assay by using the Make Your Own "Mate & Plate" Library System (Takara Bio) following the user manual. Yeast strains containing the appropriate bait and prey plasmids were cultured in liquid 2-dropout medium (leucine$^-$ and tryptophan$^-$) overnight. The overnight yeast culture was diluted to an OD600 of 0.06 and spotted on selection plates (containing histidine$^-$, leucine$^-$, tryptophan$^-$ for growth assay.

For the interaction analysis between Pha21 and Pha13, full-length Pha13 fragment was amplified by PCR with primer pair NdeI-Pha13-F/EcoR1-Pha13-R (Table 1). The Pha13 fragments were cloned into pGBKT7 and pGADT7 vector to generate pGBKT7-Pha13 as the bait vector and pGADT7-Pha13 as the prey vector. The full-length of Pha21 previously used to generate the pGBKT7-Pha21 (described above) was also cloned into pGADT7 to generate pGADT7-Pha21 as prey vector. The pGBKT7-Pha21, pGBKT7-Pha13, pGADT7-Pha21, and pGADT7-Pha13 were co-transformed into AH109 yeast strain for yeast two-hybrid assay as described above. The pGBKT7-53 and pGADT7-T from the Matchmaker Gold Yeast Two-Hybrid System kit were used as a positive control.

Accession numbers

Pha21 (PATC144963)，Pha13 (PATC148746)，PhaPR1 (PATC126136)，PhaNPR1 (PATC135791)，PhadR1 (PATC143146)，PhaRdR2 (PATC124544)，PhaRdR6 (PATC131836)，PhaDCL2 (PATC143544)，PhaDCL4 (PATC150652)，PhaAGO1 (PATC157237)，PhaAGO10 (PATC093469)，PhaGRXC9 (PATC068819)，PhaUBQ10 (PATC230548)，PhaJAZ1 (PATC141437)，PhaACO2 (PATC139319)，

AtActin (At3G18780)，AtSAP5 (AT3G12630)，DCL4 (AT5G20320)，AGO1 (AT1G48410)，OsSAP3 (LOC_Os01g56040.1)，OsSAP5 (LOC_Os02g32840.1)

ACKNOWLEDGMENTS.

We thank Shu-Chen Shen from the Confocal Microscope Core Facility at Academia Sinica for assistance in confocal microscopy images and Chii-Gong Tong from the Gene Transgenic Room at Academia Sinica for orchid transformation. This work was supported by grants from Academia Sinica, Taipei, Taiwan and the Ministry of Science and Technology (105-2313-B-001-004-MY3) of Taiwan. The funders had no role in study design, data collection and interpretation, or the decision to submit the work for publication

References

1. Pieterse CM, Leon-Reyes A, Van der Ent S, Van Wees SC. 2009. Networking by small-molecule hormones in plant immunity. Nat Chem Biol 5:308-16.
2. White R. 1979. Acetylsalicylic acid (aspirin) induces resistance to tobacco mosaic virus in tobacco. Virology 99:410-412.
3. Chivasa S, Murphy AM, Naylor M, Carr JP. 1997. Salicylic acid interferes with tobacco mosaic virus replication via a novel salicylhydroxamic acid-sensitive mechanism. The Plant Cell 9:547-557.
4. Fu ZQ, Dong X. 2013. Systemic acquired resistance: turning local infection into global defense. Annual review of plant biology 64:839-863.
5. Ausubel FM. 2005. Are innate immune signaling pathways in plants and animals conserved? Nature Immunology 6:973-979.
6. Boller T, Felix G. 2009. A renaissance of elicitors: perception of microbe-associated molecular patterns and danger signals by pattern-recognition receptors. Annual review of plant biology 60:379-406.
7. Jones JD, Dangl JL. 2006. The plant immune system. Nature 444:323-329.
8. Yang H, Gou X, He K, Xi D, Du J, Lin H, Li J. 2010. BAK1 and BKK1 in Arabidopsis thaliana confer reduced susceptibility to turnip crinkle virus. European journal of plant pathology 127:149-156.
9. Kørner CJ, Klauser D, Niehl A, Domínguez-Ferreras A, Chinchilla D, Boller T, Heinlein M, Hann DR. 2013. The immunity regulator BAK1 contributes to resistance against diverse RNA viruses. Molecular plant-microbe interactions 26:1271-1280.
10. Niehl A, Wyrsch I, Boller T, Heinlein M. 2016. Double-stranded RNAs induce a pattern-triggered immune signaling pathway in plants. New Phytologist 211:1008-1019.
11. Holmes FOJBG. 1929. Local lesions in tobacco mosaic. 87:39-55.
12. HoLMEs FOJP. 1937. Inheritance of resistance to tobacco-mosaic disease in the pepper (Capsicum sp.). 27:637-642.
13. Holmes FOJP. 1938. Inheritance of resistance to tobacco-mosaic disease in tobacco. 28.
14. Holmes FO. 1954. Inheritance of resistance to viral diseases in plants, p 1-30, Advances in virus research, vol 2. Elsevier.
15. Tsuda K, Katagiri FJCoipb. 2010. Comparing signaling mechanisms engaged in pattern-triggered and effector-triggered immunity. 13:459-465.
16. Ross AFJV. 1961. Localized acquired resistance to plant virus infection in hypersensitive hosts. 14:329-339.
17. Ross AFJV. 1961. Systemic acquired resistance induced by localized virus

711 infections in plants. 14:340-358.
712 18. Ding S-W, Voinnet O. 2007. Antiviral immunity directed by small RNAs. Cell
713 130:413-426.
714 19. Zhang C, Wu Z, Li Y, Wu J. 2015. Biogenesis, function, and applications of virus-
715 derived small RNAs in plants. Frontiers in microbiology 6:1237.
716 20. Sharma N, Sahu PP, Puranik S, Prasad MJMb. 2013. Recent advances in plant–
717 virus interaction with emphasis on small interfering RNAs (siRNAs). 55:63-77.
718 21. Blevins T, Rajeswaran R, Shivaprasad PV, Beknazariants D, Si-Ammour A, Park
719 H-S, Vazquez F, Robertson D, Meins Jr F, Hohn TJNar. 2006. Four plant Dicers
720 mediate viral small RNA biogenesis and DNA virus induced silencing.
721 34:6233-6246.
722 22. Deleris A, Gallego-Bartolome J, Bao J, Kasschau KD, Carrington JC, Voinnet OJS.
723 2006. Hierarchical action and inhibition of plant Dicer-like proteins in antiviral
724 defense. 313:68-71.
725 23. Vaucheret HJTips. 2008. Plant argonautes. 13:350-358.
726 24. Carbonell A, Carrington JCJCoipb. 2015. Antiviral roles of plant ARGONAUTES.
727 27:111-117.
728 25. Yu D, Fan B, MacFarlane SA, Chen Z. 2003. Analysis of the involvement of an
729 inducible Arabidopsis RNA-dependent RNA polymerase in antiviral defense.
730 Molecular Plant-Microbe Interactions 16:206-216.
731 26. Yang S-J, Carter SA, Cole AB, Cheng N-H, Nelson RS. 2004. A natural variant of
732 a host RNA-dependent RNA polymerase is associated with increased
733 susceptibility to viruses by Nicotiana benthamiana. Proceedings of the National
734 Academy of Sciences of the United States of America 101:6297-6302.
735 27. Liu Y, Gao Q, Wu B, Ai T, Guo X. 2009. NgRDR1, an RNA-dependent RNA
736 polymerase isolated from Nicotiana glutinosa, was involved in biotic and
737 abiotic stresses. Plant Physiology and Biochemistry 47:359-368.
738 28. Li Y, Muhammad T, Wang Y, Zhang D, Crabbe MJC, Liang YJPJOB. 2018. Salicylic
739 acid collaborates with gene silencing to tomato defense against tomato yellow
740 leaf curl virus (TYLCV).
741 29. Campos L, Granell P, Tárraga S, López-Gresa P, Conejero V, Bellés JM, Rodrigo I,
742 Lisón PJPp, biochemistry. 2014. Salicylic acid and gentisic acid induce RNA
743 silencing-related genes and plant resistance to RNA pathogens. 77:35-43.
744 30. Alamillo JM, Saénz P, García JAJTPJ. 2006. Salicylic acid-mediated and RNA-
745 silencing defense mechanisms cooperate in the restriction of systemic spread
746 of plum pox virus in tobacco. 48:217-227.
747 31. Xie Z, Fan B, Chen C, Chen Z. 2001. An important role of an inducible RNA-
748 dependent RNA polymerase in plant antiviral defense. Proceedings of the

National Academy of Sciences 98:6516-6521.

32. Hunter LJR, Westwood JH, Heath G, Macaulay K, Smith AG, MacFarlane SA, Palukaitis P, Carr JP. 2013. Regulation of RNA-dependent RNA polymerase 1 and isochorismate synthase gene expression in Arabidopsis. PLoS ONE 8:e66530.

33. Zhou M, Wang W, Karapetyan S, Mwimba M, Marqués J, Buchler NE, Dong XJN. 2015. Redox rhythm reinforces the circadian clock to gate immune response. 523:472.

34. Mou Z, Fan W, Dong X. 2003. Inducers of plant systemic acquired resistance regulate NPR1 function through redox changes. Cell 113:935-944.

35. Tada Y, Spoel SH, Pajerowska-Mukhtar K, Mou Z, Song J, Wang C, Zuo J, Dong X. 2008. Plant immunity requires conformational charges of NPR1 via S-nitrosylation and thioredoxins. Science 321:952-956.

36. Herrera-Vásquez A, Salinas P, Holuigue LJFips. 2015. Salicylic acid and reactive oxygen species interplay in the transcriptional control of defense genes expression. 6:171.

37. Cao H, Bowling SA, Gordon AS, Dong X. 1994. Characterization of an Arabidopsis mutant that is nonresponsive to inducers of systemic acquired resistance. The Plant Cell 6:1583-1592.

38. Delaney T, Friedrich L, Ryals J. 1995. Arabidopsis signal transduction mutant defective in chemically and biologically induced disease resistance. Proceedings of the National Academy of Sciences 92:6602-6606.

39. Shah J, Tsui F, Klessig DF. 1997. Characterization of a s alicylic a cid-i nsensitive mutant (sai1) of Arabidopsis thaliana, identified in a selective screen utilizing the SA-inducible expression of the tms2 gene. Molecular Plant-Microbe Interactions 10:69-78.

40. Wong CE, Carson RA, Carr JP. 2002. Chemically induced virus resistance in Arabidopsis thaliana is independent of pathogenesis-related protein expression and the NPR1 gene. Molecular plant-microbe interactions 15:75-81.

41. Kachroo P, Yoshioka K, Shah J, Dooner HK, Klessig DF. 2000. Resistance to turnip crinkle virus in Arabidopsis is regulated by two host genes and is salicylic acid dependent but NPR1, ethylene, and jasmonate independent. The Plant Cell 12:677-690.

42. Vij S, Tyagi AK. 2008. A20/AN1 zinc-finger domain-containing proteins in plants and animals represent common elements in stress response. Functional & integrative genomics 8:301-307.

43. Giri J, Dansana PK, Kothari KS, Sharma G, Vij S, Tyagi AK. 2013. SAPs as novel regulators of abiotic stress response in plants. Bioessays 35:639-648.

44. Chang L, Chang H-H, Chang J-C, Lu H-C, Wang T-T, Hsu D-W, Tzean Y, Cheng A-P,

Chiu Y-S, Yeh H-HJPp. 2018. Plant A20/AN1 protein serves as the important hub to mediate antiviral immunity. 14:e1007288.

45. Kang M, Fokar M, Abdelmageed H, Allen RD. 2011. Arabidopsis SAP5 functions as a positive regulator of stress responses and exhibits E3 ubiquitin ligase activity. Plant molecular biology 75:451-466.

46. Kang M, Lee S, Abdelmageed H, Reichert A, Lee HK, Fokar M, Mysore KS, Allen RD. 2017. Arabidopsis stress associated protein 9 mediates biotic and abiotic stress responsive ABA signaling via the proteasome pathway. Plant, cell & environment 40:702-716.

47. Choi H, Han S, Shin D, Lee S. 2012. Polyubiquitin recognition by AtSAP5, an A20-type zinc finger containing protein from Arabidopsis thaliana. Biochemical and biophysical research communications 419:436-440.

48. Verhelst K, Carpentier I, Kreike M, Meloni L, Verstrepen L, Kensche T, Dikic I, Beyaert R. 2012. A20 inhibits LUBAC-mediated NF-κB activation by binding linear polyubiquitin chains via its zinc finger 7. The EMBO Journal 31:3845-3855.

49. Wertz IE, O'rourke KM, Zhou H, Eby M. 2004. De-ubiquitination and ubiquitin ligase domains of A20 downregulate NF-kappaB signalling. Nature 430:694.

50. Mattera R, Tsai YC, Weissman AM, Bonifacino JS. 2006. The Rab5 guanine nucleotide exchange factor Rabex-5 binds ubiquitin (Ub) and functions as a Ub ligase through an atypical Ub interacting motif and a zinc finger domain. The Journal of Biological Chemistry 281:6874-6883.

51. Lu HC, Hsieh MH, Chen CE, Chen HH, Wang HI, Yeh HH. 2012. A high-throughput virus-induced gene-silencing vector for screening transcription factors in virus-induced plant defense response in orchid. Molecular Plant-Microbe Interactions 25:738-746.

52. Chang C-H, Wang H-I, Lu H-C, Chen C-E, Chen H-H, Yeh H-H, Tang CY. 2012. An efficient RNA interference screening strategy for gene functional analysis. BMC genomics 13:491.

53. Ma A, Malynn BA. 2012. A20: linking a complex regulator of ubiquitylation to immunity and human disease. Nature reviews Immunology 12:774.

54. Hishiya A, Iemura Si, Natsume T, Takayama S, Ikeda K, Watanabe K. 2006. A novel ubiquitin-binding protein ZNF216 functioning in muscle atrophy. The EMBO Journal 25:554-564.

55. Miyata N, Okumoto K, Mukai S, Noguchi M, Fujiki Y. 2012. AWP1/ZFAND6 Functions in Pex5 Export by Interacting with Cys-Monoubiquitinated Pex5 and Pex6 AAA ATPase. Traffic 13:168-183.

56. Giri J, Vij S, Dansana PK, Tyagi AK. 2011. Rice A20/AN1 zinc-finger containing stress-associated proteins (SAP1/11) and a receptor-like cytoplasmic kinase

(OsRLCK253) interact via A20 zinc-finger and confer abiotic stress tolerance in transgenic Arabidopsis plants. New Phytologist 191:721-732.

57. Karimi M, Inzé D, Depicker A. 2002. GATEWAY™ vectors for Agrobacterium-mediated plant transformation. Trends in plant science 7:193-195.

58. Hsing H-X, Lin Y-J, Tong C-G, Li M-J, Chen Y-J, Ko S-S. 2016. Efficient and heritable transformation of Phalaenopsis orchids. Botanical studies 57:30.

59. Wu H-Y, Liu K-H, Wang Y-C, Wu J-F, Chiu W-L, Chen C-Y, Wu S-H, Sheen J, Lai E-M. 2014. AGROBEST: an efficient Agrobacterium-mediated transient expression method for versatile gene function analyses in Arabidopsis seedlings. Plant methods 10:19.

FIGURE LEGENDS:

FIG 1 Sequence and expression analysis of Pha21 (A) A schematic representation of domain organization of Pha21. The open rectangle indicates the entire protein. A20 (dark grey rectangle) and AN1 (light grey rectangle) and 21-nucleotide position (short black line) used for designing hairpin RNA of Pha21 (hpPha21-1 and hpPha21-2) are indicated. (B) Amino sequence alignment of A20/AN1 zinc finger domains of Pha21 with stress-associated proteins from *Phalaenopsis aphrodite* (Pha13, accession number: PATC148746), *Arabidopsis thaliana* (AtSAP5, accession number: AT3G12630), and *Oryza sativa* (OsSAP3, accession number: LOC_Os01g56040.1; OsSAP5, accession number: LOC_Os02g32840.1) is shown. The black box indicates the conserved amino acid sequences. The black triangle indicates the conserved cysteine (C) and histidine (H) residues. (C) Primary sequence organization of A20 and AN1 domains. Xn: the number of amino acid residues between zinc ligands. (B-C) The mutation positions for domain functional analysis are indicated with a blue triangle. (D) Expression level of *Pha21* was analyzed by qRT-PCR from the root, leaf, petal, sepal, column, and lip of *P. aphrodite*. The RNA level of the root was set to 1. Data represent mean ± SD; n = 3 technical replicates; different letters indicate statistically significant differences analyzed by one-way analysis of variance (ANOVA) Tukey's test ($P < 0.05$). The experiment was repeated at least three times with similar results, and one representative

854 experiment is shown. *PhaUbiquitin 10* was used as an internal control for normalization.
855 (E) Absolute quantitative analysis of *Pha13* and *Pha21* expression. The mRNA copy
856 numbers of Pha13 and Pha21 in leaves of *P. aphrodite* were absolutely quantified by
857 droplet digital PCR. Total RNA (ng) was used for normalization. Data represent mean
858 ± SD; n = 3 biological replicates; **, $P < 0.01$, Student's t test compared Pha13 with
859 Pha21
860
861 **FIG 2** Pha21 is involved in the expression of *PhaPR1* and *PhaNPR1,* and responds to
862 phytohormone treatment. (A-B) qRT-PCR was performed to quantify the expression
863 level of *Pha21*, *PhaNPR1*, and *PhaPR1* from leaves of *P. aphrodite* infiltrated with
864 agrobacterium carrying control vector (Vector); hairpin RNA vector to knock down
865 Pha21 (hpPha21-1 and hpPha21-2; A); and overexpression vector of Pha21 (Pha21-oe;
866 B). The expression level of plants infiltrated with control vector was set to 1. (C)
867 Transient silencing of PhaNPR1. qRT-PCR was performed to quantify the expression
868 level of *PhaNPR1*, *PhaPR1*, and *Pha21* from leaves of *P. aphrodite* infiltrated with
869 agrobacterium carrying control vector (Vector) or hairpin RNA (hpRNA) vector to
870 knock down PhaNPR1 (hpPhaNPR1). The expression level of plants infiltrated with
871 control vector was set to 1. (A-C) Data represent mean ± SD; n = 3 biological replicates;
872 **, $P < 0.01$; *, $P < 0.05$, Student's t test compared to Vector. (D-F) Time-course
873 expression of *Pha21* under different plant hormone treatments in *P. aphrodite*. qRT-
874 PCR was performed to analyze the expression level of *Pha21* from leaves treated with
875 SA (D), JA (E), and ET (F) at different hours (h) post-treatment. Buffer treatment was
876 used as a mock control. Results of qRT-PCR were relative to that of mock at individual
877 time courses for relative quantification. The expression level at 0 h was set to 1 for
878 comparison between different time courses. *PhaPR1* and *PhaNPR1* were SA-
879 responsive marker genes. *PhaJAZ1* and *PhaACO2* were JA and ET–responsive marker

880 genes, respectively. Data represent mean ± SD; n = 3 biological replicates; **, $P < 0.01$;
881 *, $P < 0.05$, Student's t test compared to 0 h. (A-F) *PhaUbiquitin 10* was used as an
882 internal control for normalization.
883
884 **FIG3** Pha21 is involved in virus accumulation. (A) qRT-PCR was performed to
885 quantify the CymMV accumulation level and expression level of *Pha21* in healthy
886 (Mock) and CymMV-infected (Cy-infected) *P. aphrodite.* The expression level in the
887 CymMV-infected (Cy-infected) *P. aphrodite* was set to 1. Data represent mean ± SD; n
888 = 3 biological replicates; **, $P < 0.01$; *, $P < 0.05$, Student's t test compared to mock.
889 (B-C) Transient silencing or overexpression of Pha21 in CymMV-infected plants. qRT-
890 PCR was performed to quantify the expression level of *Pha21* and CymMV
891 accumulation level from leaves of CymMV-infected *P. aphrodite* infiltrated with
892 agrobacterium carrying vector (Vector); hairpin RNA (hpRNA) vector to knockdown
893 Pha21 (hpPha21-1 and hpPha21-2; B); or overexpression vector of Pha21 (Pha21-oe;
894 C). The expression level of plants infiltrated with control vector was set to 1. Data
895 represent mean ± SD; n = 3 biological replicates; **, $P < 0.01$; *, $P < 0.05$, Student's t
896 test compared to Vector. (D) The wild-type (WT) *P. equestris* orchid and transgenic *P.*
897 *equestris* (Pha21#8 and #9) were used for analysis. expression level of *Pha21* and
898 CymMV were analyzed by qRT-PCR from leaves of WT or transgenic *P. equestris*
899 (Pha21#8 and #9) inoculated with CymMV. The expression level of WT was set to 1.
900 Data represent mean ± SD; n = 2 biological replicates; **, $P < 0.01$; *, $P < 0.05$,
901 Student's t-test compared to WT. (A-D) *PhaUbiquitin 10* was used as an internal
902 control for normalization.
903
904 **FIG4** Overexpression of Pha21 in engineered transgenic *Arabidopsis* enhances
905 resistance against viruses. (A) Expression level of *Pha21* and accumulation level of

906 *Cucumber mosaic virus* (CMV) were analyzed by qRT-PCR from leaves of WT (Col-
907 0) or transgenic *Arabidopsis* (At-Pha21#4, #5, and #6). Data represent mean ± SD; n =
908 5 biological replicates; **, $P < 0.01$; *, $P < 0.05$, Student's t-test compared to WT.
909 *AtActin* was used as an internal control for normalization. (B) Disease symptoms of WT
910 (Col-0) or transgenic *Arabidopsis* (At-Pha21#4, #5, and #6) inoculated with CMV at
911 14 dpi. Images are one representative plant from five replicates; Scale bar, 1 cm.
912
913 **FIG 5** Subcellular localization of Pha21 and transcriptional activation analysis of
914 Pha13 and Pha21. (A) Green fluorescent protein (GFP) or N- and C- terminal GFP-
915 fused Pha21 (G-Pha21 and Pha21-G) were co-transfected with nucleus localization
916 signal fused red fluorescence protein (NLS-RFP) into protoplasts of *P. aphrodite*.
917 Fluorescence was detected by confocal microscopy after transfection. Scale bars
918 represent 10 μm. (B) Yeast two-hybrid assay was used to analyze the transcriptional
919 activation. AH109 is the yeast strain used in this assay. The pGBKT7-Pha13 and
920 pGBKT7-Pha21 indicates that yeast encodes Pha13 or Pha21 fused to the Gal4 DNA
921 binding domain. The pGBKT7-53, pGADT7-T, and pGBKT7-Lam provided in
922 Matchmaker Gold Yeast Two-Hybrid System kit were used as a positive (pGBKT7-53
923 + pGADT7-T) and negative (pGBKT7-Lam + pGADT7-T) control. The -Trp indicates
924 the medium without tryptophan. The -Trp/Aureobasidin was used to test for activation
925 of the inositol phosphoryl ceramide synthase (AUR1-C) for Aureobasidin A resistance.
926 The -Trp/X-α-Gal medium was used to test for activation of α-galactosidase, and -Trp/-
927 Ade/-His indicate the selective medium without tryptophan, adenine, and histidine
928
929 **FIG 6** Pha21 confers self-ubiquitination E3 ligase activity and ubiquitin binding ability.
930 (A) The *in vitro* self-ubiquitination E3 ligase activity assay was conducted on wild-type
931 Pha21, A20 mutant (Pha21-A20m), AN1 mutant (Pha21-AN1m), A20/AN1 double

mutant (Pha21-A20mAN1m) with or without FLAG-Ub, human ubiquitin-activating enzyme (hE1), or human ubiquitin-conjugating enzyme (hE2). Coomassie staining for Pha21 was used as a loading control. Ubiquitinated proteins were analyzed with immunoblotting using anti-FLAG antibodies. The ubiquitinated Pha21 are indicted as Pha21-Ub. E1 conjugated with one Ub (E1-Ub), E2 conjugated with one or two Ub (E2-Ub, E2-2Ub), and free Ub are indicated with a black arrow. (B) Yeast two-hybrid assay was performed to analyze the interaction between full-length and deletion mutant of Pha21 and ubiquitin. The schematic representations of full-length and deletion mutant of Pha21 are indicated. The open rectangle indicates the entire Pha21 protein. A20 domain and AN1 domain are indicated as a dark blue oval circle and a light blue oval circle, respectively. The full-length and deletion mutant of Pha21 cloned in pGBKT7 vector were co-transformed with pGADT7-PhaUBQ into yeast AH109 strain. The 2DO indicates the Leucine and Trptophan dropout selective medium and 3DO indicates the Leucine, Trptophan, and Histidine dropout selective medium. The pGBKT7 was used as a negative control.

FIG 7 Interaction analysis of Pha21 and Pha13. Yeast two-hybrid assay was performed to analyze the interaction between Pha21 and Pha13. The pGBKT7 and pGADT7 were used as a negative control. The pGBKT7-53 and pGADT7-T (provided in the Matchmaker Gold Yeast Two-Hybrid System kit), and pGBKT7-Pha21 and pGADT7-PhaUBQ were used as a positive control. The 2DO indicates the dropout selective medium without Leucine and Tryptophan. The 3DO indicates dropout selective medium without the Leucine, Tryptophan, and Histidine.

FIG 8 Pha21 is involved in the expression of PhaNPR1-dependent gene, *PhaRdR1,* and PhaNPR1-independent gene, *PhaGRXC9*. The expression levels of *Pha21, PhaRdR1*,

958 and *PhaGRXC9* were analyzed by qRT-PCR from leaves of *P. aphrodite* infiltrated with
959 agrobacterium carrying control vector (Vector) or hairpin RNA (hpRNA) vector to
960 knockdown Pha21 (hpPha21-2; A), or to overexpress Pha21 (Pha21-oe; B). The RNA
961 level of plants infiltrated with control vector was set to 1. Data represent mean ± SD; n
962 = 3 biological replicates; **, $P < 0.01$; *, $P < 0.05$, Student's t-test compared to Vector.
963 (A-B) *PhaUbiquitin 10* was used as an internal control for normalization.
964
965 **FIG 9** Pha21 is involved in the expression of *PhaDCL4* and *PhaAGO1*. (A-C) The
966 expression levels of *Pha13*, *Pha21*, *PhaRdR2*, *PhaRdR6*, *PhaDCL2*, *PhaDCL4*,
967 *PhaAGO1*, and *PhaAGO10* were analyzed by qRT-PCR from leaves of *P. aphrodite*
968 infiltrated with agrobacterium carrying control vector (Vector); overexpression vector
969 of Pha21 (Pha21-oe; A); hairpin RNA vector to knock down Pha21 (hpPha21-2; B);
970 and overexpression vector of Pha13 (Pha13-oe; C). The expression level of plants
971 infiltrated with control vector was set to 1. Data represent mean ± SD; n = 3 biological
972 replicates; **, $P < 0.01$; *, $P < 0.05$, Student's t-test compared to Vector. (D-E) The
973 expression level of *PhaDCL4*, *PhaAGO1*, and CymMV accumulation level were
974 analyzed by qRT-PCR from leaves of CymMV-infected *P. aphrodite* infiltrated with
975 agrobacterium carrying vector (Vector); hairpin RNA (hpRNA) vector to knock down
976 PhaDCL4 (hpPhaDCL4, D), or PhaAGO1 (hpPhaAGO1, E). The expression level of
977 plants infiltrated with control vector was set to 1. Data represent mean ± SD; n = 3
978 biological replicates; **, $P < 0.01$; *, $P < 0.05$, Student's t test compared to Vector. (A-
979 E) *PhaUbiquitin 10* was used as an internal control for normalization.
980
981 **FIG 10** AtSAP5 is involved in the expression of *DCL4* and *AGO1*. (A-C) The
982 expression levels of *AtSAP5, DCL4, AGO1* were analyzed by qRT-PCR in WT,
983 AtSAP5 overexpression (AtSAP5-oe-4 and AtSAP5-oe-11) and RNAi lines

(AtSAP5-RNAi-3 and AtSAP5-RNAi-7). Data represent mean ± SD; n = 5 biological replicates; **, $P < 0.01$; *, $P < 0.05$, Student's t-test. Student's t test compared to WT. *AtActin* was used as an internal control for normalization.

FIG 11 Pha21 A20 and AN1 domain play different roles in the expression of *PhaDCL4, PhaAGO1, PhaGRXC9* and virus resistance. The expression level of *Pha21*, *PhaDCL4, PhaAGO1*, *PhaGRXC9* and CymMV accumulation level were analyzed by qRT-PCR in leaves of healthy *P. aphrodite* (A), or CymMV pre-infected *P. aphrodite* (B) infiltrated with agrobacterium carrying control vector (Vector), overexpression clones of Pha21 (Pha21-oe), or the respective A20 and/or AN1 mutant clones (Pha21A20m, Pha21AN1m, and Pha21A20mAN1m). The RNA level of plants infiltrated with control vector was set to 1. Data represent mean ± SD; n = 3 biological replicates; **, $P < 0.01$; *, $P < 0.05$; ns, no significant difference, Student's t test compared to Vector. (A-B) *PhaUbiquitin 10* was used as an internal control for normalization.

FIG 12 The role of A20/AN1 proteins in antiviral immunity.

A model illustrating the roles of SA-induced-A20/AN1 proteins Pha13 and Pha21 from *Phalaenopsis aphrodite,* and AtSAP5 from *Arabidopsis thaliana* in antiviral immunity. Virus infection caused accumulation of SA and led to the activation of *Pha13*, *Pha21*, and *AtSAP5*, allowing it to trigger the SA-and RNAi-mediated immune responsive genes including *NPR1*, *GRXC9*, *DCL4*, *AGO1*, and *RdR1* in antiviral immunity.

1006 **Table 1.** Primers and probes used in this study

Name of primers and probes	Nucleotide sequence	Description
Semi-quantitative RT-PCR		
CymMV-F	5'-GAAATAATCATGGGAGAGCC-3'	Detection of *Cymbidium mosaic virus* (CymMV)
CymMV-R	5'-AGTTTGGCGTTATTCAGTAGG-3'	
ORSV-F	5'-ACGCACAATCTGATCCGTA-3'	Detection of *Odontoglossum ringspot virus* (ORSV)
ORSV-R	5'-ATCCGCAGTGAAAACCC-3'	
Real-time RT-PCR		
Pha13-qF	5'-TCATCTTAAAACAGAGCAGGATCTGA-3'	Detection of *Pha13* (PATC148746[a])
Pha13-qR	5'-CGGCGTCTAAAGAAGAGGAAGAG-3'	
Pha21-qF	5´-CCATCTTAAAACCCAGGATGCT-3´	Detection of *Pha21* (PATC144963[a])
Pha21-qR	5´-TGGAGTCGACGAGGAACAGAA-3´	
PhaNPR1-qF	5'-AGTTGATGGCACCTTGGAGTTT-3'	Detection of *PhaNonexpressor of pathogenesis-related gene 1* (*PhaNPR1*; PATC135791[a])
PhaNPR1-qR	5'-AAGAAGCGTTTCCCGAGTTCA-3'	
PhaPR1-qF	5'-GGATCATCGTCTTGCGATTT-3'	Detection of *PhaPathogenesis-related gene 1* (*PhaPR1*; PATC126136[a])
PhaPR1-qR	5'-CCGCACAACTGTTACATGCAT-3'	
CymMV-qF	5'-TGATGCTGGCCACTAACGATC-3'	Detection of CymMV
CymMV-qR	5'-GGAATCAACGGCATCGAAGA-3'	
PhaRdR1-qF	5'-TGACAAGTACAAGGATGGCG-3'	Detection of *PhaRNA-dependent RNA polymerase 1* (*PhaRdR1*; PATC143146[a])
PhaRdR1-qR	5'-ACTCTTCACCCCATCAACATC-3'	
PhaRdR2-qF	5'-AAAATCCTTGTCTCCACCCTG-3'	Detection of *PhaRdR2* (PATC124544[a])
PhaRdR2-qR	5'-GCAATCTACGAGTCCCATCTC-3'	
PhaRdR6-qF	5'-AGAGCTGGGAATGGAAGTTG-3'	Detection of *PhaRdR6* (PATC131836[a])
PhaRdR6-qR	5'-GTCGAATTTCTGCATGGTTGG-3'	
PhaDCL2-qF	5'-CATTGCATCAGAAAGCCATCG-3'	Detection of *PhaDicer-like nuclease 2* (*PhaDCL2*; PATC143544[a])
PhaDCL2-qR	5'-ACCTCAAACGTCTCCAACTTC-3'	
PhaDCL4-qF	5'-CATGACTTCGATAGGGTTGGG-3'	Detection of *PhaDCL4* (PATC150652[a])
PhaDCL4-qR	5'-GAGTTTCGCCATTCTTTGCTG-3'	
PhaAGO1-qF	5'-ACAGGAGACAAGCCAAAGAG-3'	Detection of *PhaArgonaut 1* (*PhaAGO1*; PATC157237[a])
PhaAGO1-qR	5'-ACCACAAAAGTGACGAGAGG-3'	

Table 1. Cont.

PhaAGO10-qF	5'-TGAACCAAACTACCAGCCAC-3'	Detection of *PhaAGO10*
PhaAGO10-qR	5'-TGTTTCCATTCCTGTCCGTAG-3'	(PATC093469[a])
PhaGRXC9-qF	5'-ACGTCGTAAAGCATCTCCTT-3'	Detection of *PhaGlutaredoxin C9* (PhaGRXC9; PATC068819[a])
PhaGRXC9-qR	5'-CGGTAAGGTCACCGTAAAAC-3'	
PhaUBQ 10-qF	5'-CCGGATCAGCAAAGGTTGA-3'	Detection of (PhaUBQ10;
PhaUBQ 10-qR	5'-AAGATTTGCATCCCTCCCC-3'	PATC230548[a])
PhaJAZ1-qF	5'-CTCGGAGTGGTTGGCTTTATTAG-3'	Detection of *PhaJasmonate ZIM-domain protein 1* (*PhaJAZ1*; PATC141437[a])
PhaJAZ1-qR	5'-GTGATGCCTTCCTTGCGATT-3'	
PhaACO2-qF	5'-CGTCCAAAACGCTTGATTCC-3'	Detection of *PhaAmino-cyclopropane-carboxylate oxidase 2* (*PhaACO2*; PATC139319[a])
PhaACO2-qR	5'-GCGCAAATTCCTTCATGGTT-3'	
AtACT-qF	5'-GGCAAGTCATCACGATTGG -3'	Detection of *AtActin*
AtACT-qR	5'-CAGCTTCCATTCCCACAAAC -3'	(AT3G18780)
CMV-qF	5'-TTCCTGCCTCCTCGGACTTA-3'	Detection of CMV
CMV-qR	5'-GCTCCGTCCGCGAACATA-3'	
AtSAP5-qF	5'-ACCAGCTAAAGTCGTGATTCG-3'	Detection of *AtSAP5*
AtSAP5-qR	5'-AGCGGTTTTGTAGTCGTAGC-3'	
DCL4-qF	5'-GCCCCTCACTACTCGCAATA-3'	Detection of *DCL4*
DCL4-qR	5'-GAACAGCATCCCCAAGAAA-3'	
AGO1-qF	5'- GTTTTCGCATTCAGCACACTC-3'	Detection of *AGO1*
AGO1-qR	5'-CAATCTTTTGGAATACCGCTG-3'	
Droplet digital PCR		
Pha13-ddPCR-P-FAM	5'-TCTCCACGGCGATCAGATCC-3'	FAM-labeled probe for
Pha21-ddPCR-P-FAM	5'-ATGCTCTGCTCGCTGTCGAA-3'	detection of *Pha13* or *Pha21*
Pha13-ddPCR-F	5'-AACCCTAAACCTCTGCTC-3'	Detection of *Pha13*
Pha13-ddPCR-R	5'-GAGGAGGAGGAGGAGAAG-3'	
Pha21-ddPCR-F	5'-CTGCTCTAAGTGTTACGG-3'	Detection of *Pha21*
Pha21-ddPCR-R	5'-TCGACGAGGAACAGAATA-3'	
Construction		
Pha21-hpRNA-1-F	5'-CACCTTACGGAGACCATCTTAAAAC-3'	Construction of phpPha21-1
Pha21-hpRNA-1-R	5'-GTTTTAAGATGGTCTCCGTAA-3'	
Pha21-hpRNA-2-F	5'-CACCCCAGGATGCTCTGCTCGCTGT-3'	Construction of phpPha21-2
Pha21-hpRNA-2-R	5'-ACAGCGAGCAGAGCATCCTGG-3'	

Table 1. Cont.

PhaNPR1-hpRNA-F	5' -CACCCGAGATCATTGATTCCTTCCC-3'	Construction of phpPhaNPR1
PhaNPR1-hpRNA-R	5' -GGGAAGGAATCAATGATCTCG-3'	
PhaDCL4-hpRNA-F	5'-CACCGAGAATTTACTTGATGCAAAG-3'	Construction of phpPhaDCL4
PhaDCL4-hpRNA-R	5' -CTTTGCATCAAGTAAATTCTC-3'	
PhaAGO1-hpRNA-F	5'-CACCACATGGTGGTGTGCCACAAGG-3'	Construction of phpPhaAGO1
PhaAGO1-hpRNA-R	5'-CCTTGTGGCACACCACCATGT-3'	
Pha21-ORF-F	5'-CACCATGGCGGAGGATCAGCCATG-3'	Construction of pG-Pha21 or pPha21-G
Pha21-ORF-NONSTOP-R	5'-AATTTTGTCCAGCTTCTCCGCC-3'	
FLAG-Pha21ORF-F	5'-CACCATGGATTACAAGGATGACGACGA TAAGATGGCGGAGGATCA-3'	Construction of pPha21-oe and pHPha21
Pha21ORF-R	5'-CTAAATTTTGTCCAGCTTCTCCG-3'	
Pha21A20m-F	5'-GCTACTCTCAATCTCGGCTCTAAGGGTTA CGGAGACCATC-3'	Construction of pPha21A20m
Pha21A20m-R	5'-GATGGTCTCCGTAACCCTTAGAGCCGAGA TTGAGAGTAGC-3'	
Pha21AN1m-F	5'- CTCCTTGGGTTCAAGGGTCGGTGCGGTGT GACGCACTGCGGAGACGGCCGGTACCCGGAGCA-3'	Construction of pPha21AN1m
Pha21AN1m-R	5'- TGCTCCGGGTACCGGCCGTCTCCGCAGTG GTCACACCGCACCGACCCTTGAACCCAAGGAG-3'	
NdeI-Pha21-F[b]	5'- ATTCCATATGGCGGAGGATCAGCCAT-3'	Construction of pETPha21, pETPha21A20m, pETPha21AN1m and pETPha21A20mAN1m
NotI-Pha21-R[b]	5'- ACATGCGGCCGCAATTTTGTCCAGCTTCT -3'	
NdeI-Pha21-F[b]	5'- ATTCCATATGGCGGAGGATCAGCCAT-3'	For construction of full-length and deletion mutant of Pha21 into pGBKT7 and construction of pGADT7-Pha21
NdeI-Pha21-16-F[b]	5'-CTGCATATGGACCATCTTAAAACCCAGGATGCTC-3'	
NdeI-Pha21-41-F[b]	5'-CTGCATATGGACCATCTTAAAACCCAGGATGCTC-3'	
NdeI-Pha21-102-F[b]	5'-CTGCATATGTGCCGGAAGAAGGTGGG-3'	
NdeI-Pha21-137-F[b]	5'-CTGCATATGTCGGCCAGCCGCG-3'	
BamH1-Pha21-R[b]	5'-GACGGATCCTAAATTTTGTCCAGCTTC-3'	
BamHI-Pha21-15-R[b]	5'-GACGGATCCTATTCTTGGCATCTCCGTCCC-3'	
BamHI-Pha21-40-R[b]	5'-GACGGATCCTATCCGTAACACTTAGAGCAGAGATT GAG-3'	

Table 1. Cont.

BamHI-Pha21-101-R[b]	5'-GACGGATCCTACGCCGCGCACCG-3'	
BamHI-Pha21-136-R[b]	5'-GACGGATCCTACTTGAAATCAAAGCAGCAGCC-3'	
NdeI-PhaUBQ-F[b]	5 ´ -CTCTCATATGAGGGGAGGTATGCAGATTT TCG-3'	Construction of polyubiquitin into pGADT7
BamHI-PhaUBQ-R[b]	5'-CTATGGATCCACCACGAAGACGGAGCACA A-3'	
NdeI-Pha13-F[b]	5'-AGAGCATATGGCTGCCACCTTCTCCTCCT TTT-3'	Construction of pGBKT7-Pha13 and pGADT7-Pha13
EcoR1-Pha13-R[b]	5'-AGAGGAATTCAAATCTTCCGCAGCTTA-3'	

[a]Accession number of Orchidstra database (http://orchidstra.abrc.sinica.edu.tw)

[b]Underlined sequences indicate the sequence recognized by restriction enzyme. The random 4 nucleotides at the 5' end were added as recommended by the manufactur

1014 **FIG 1**

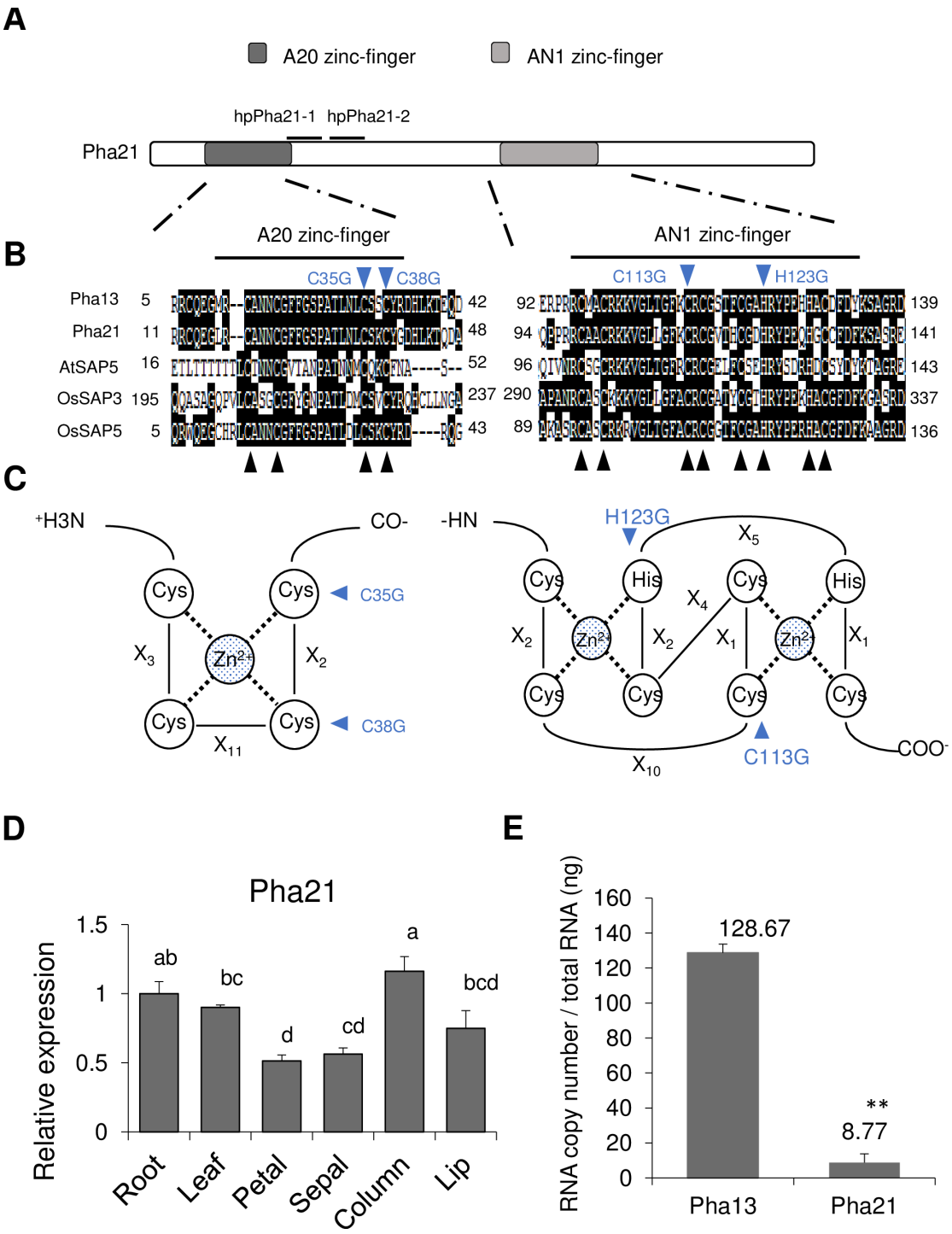

1015

1016

1017

1018 **FIG 2**

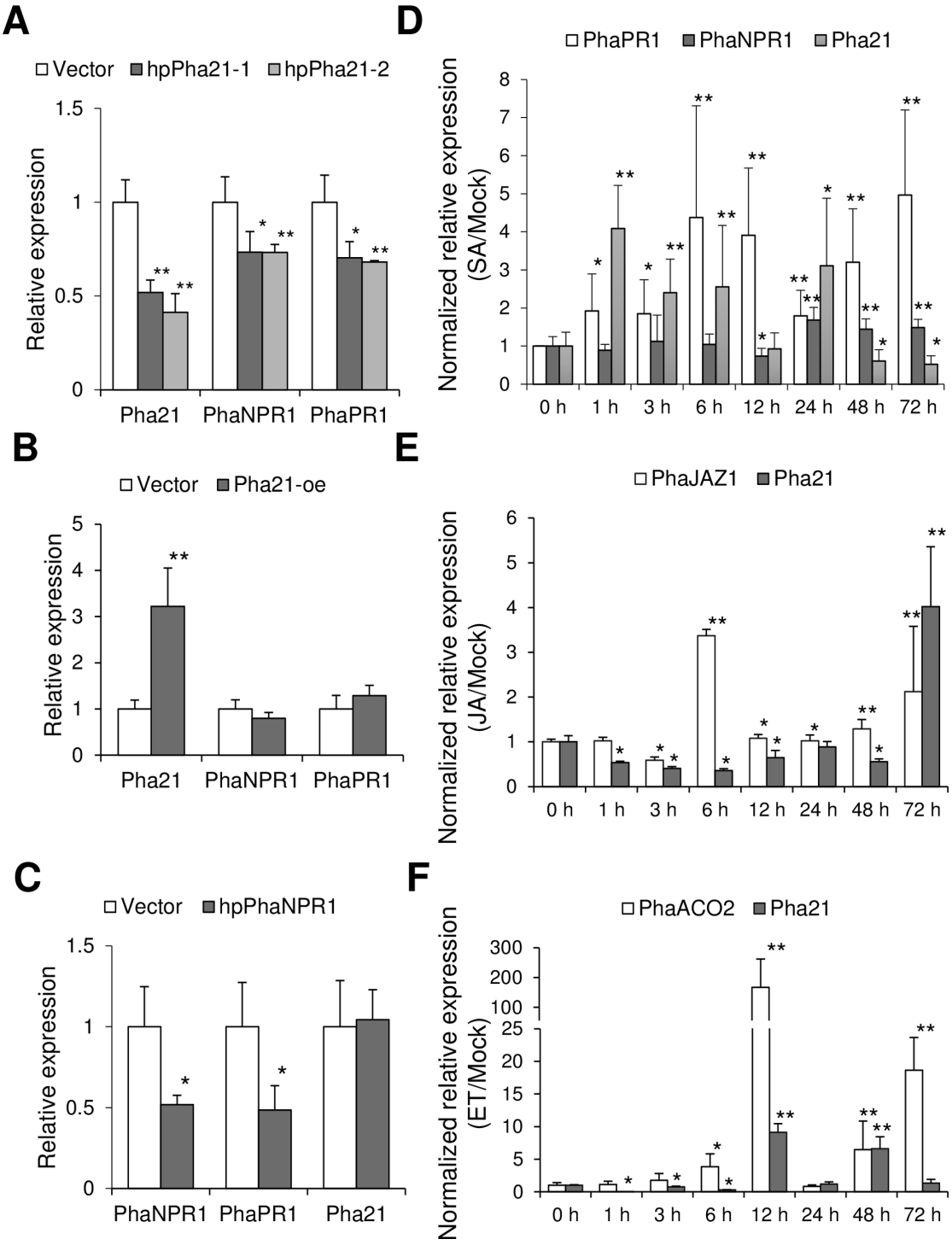

1019

1020

1021

1022 **FIG 3**

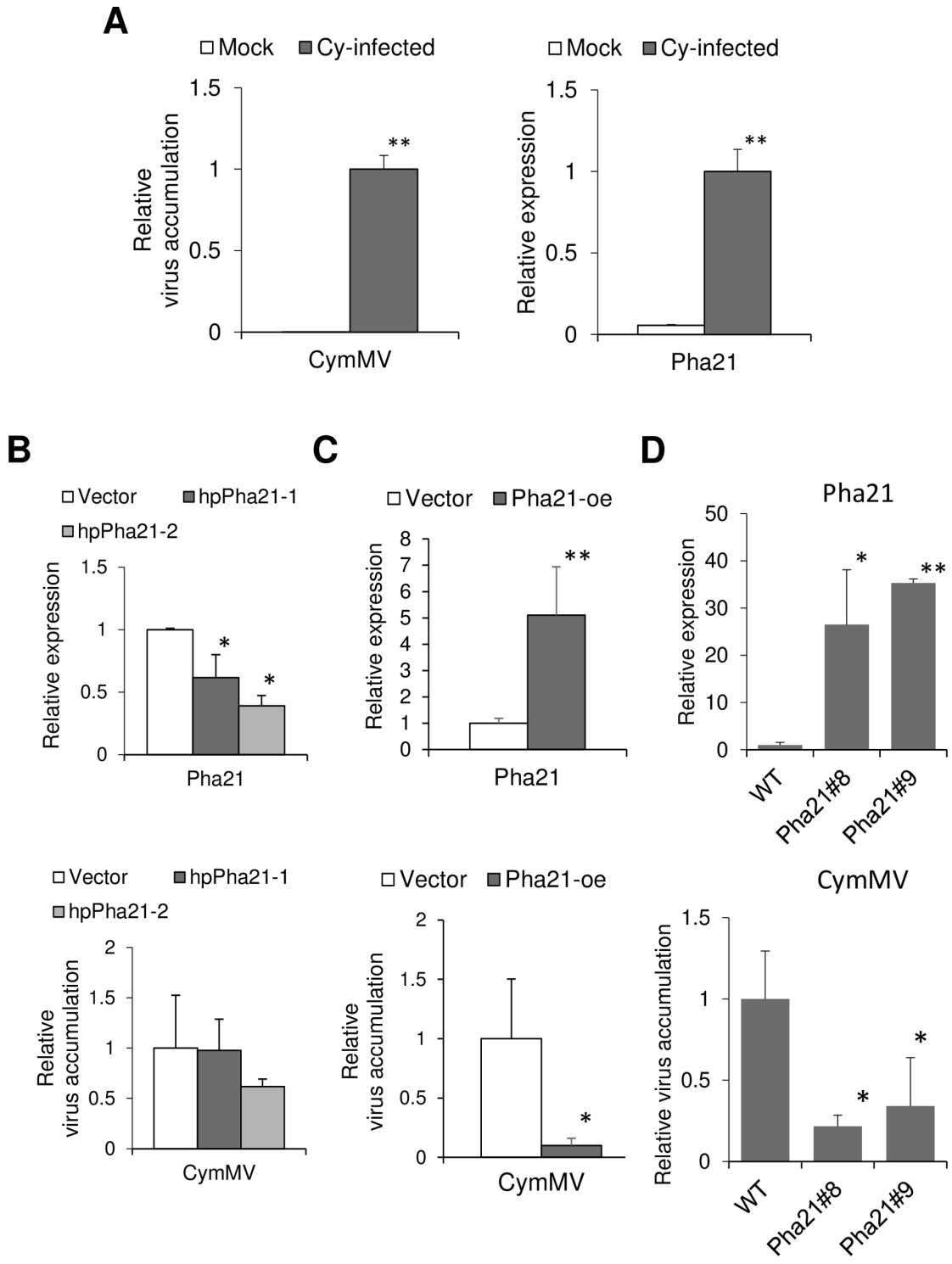

1023

1024

1025

1026 **FIG 4**

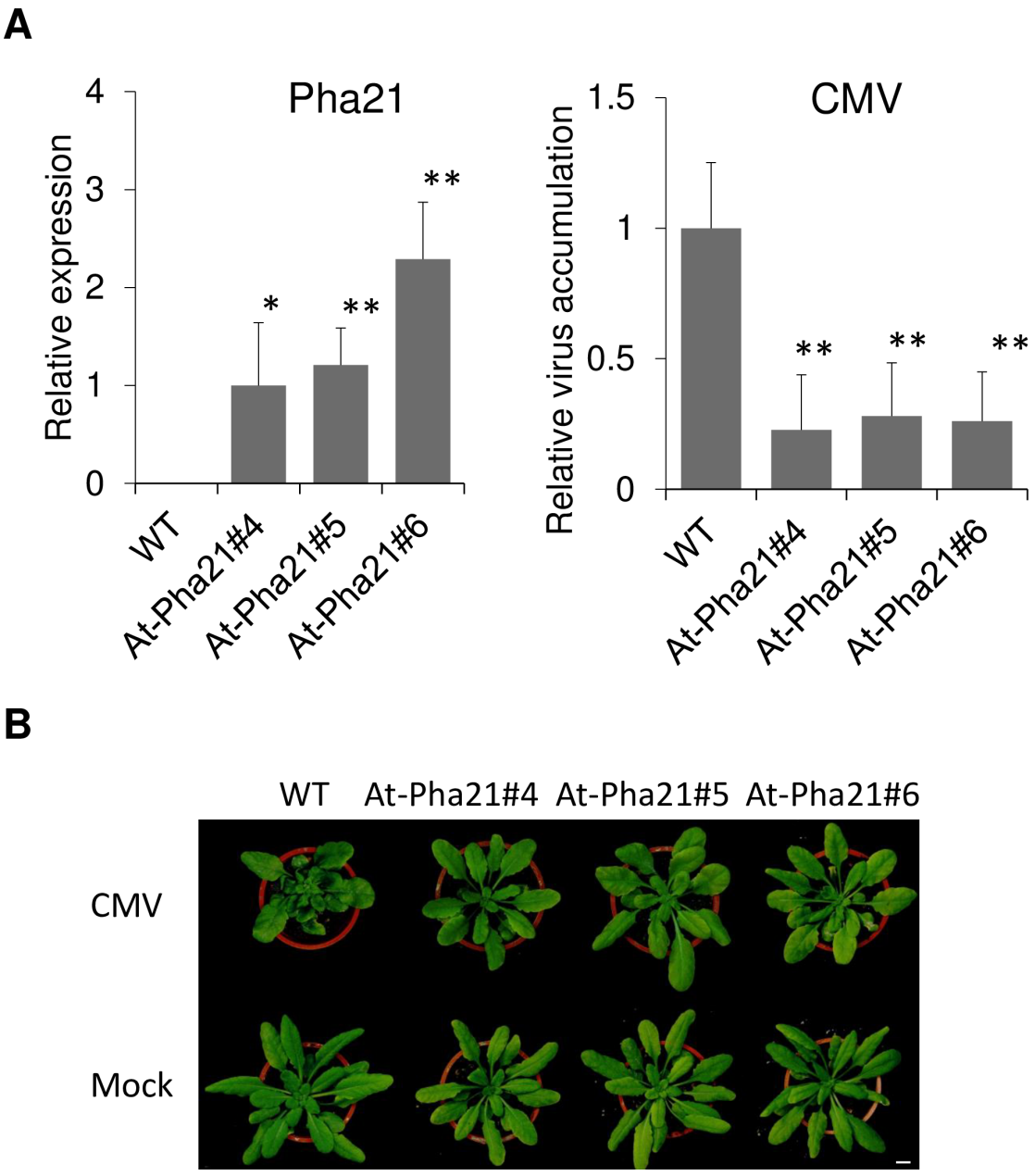

1027

1028

1029

1030

1031 **FIG 5**

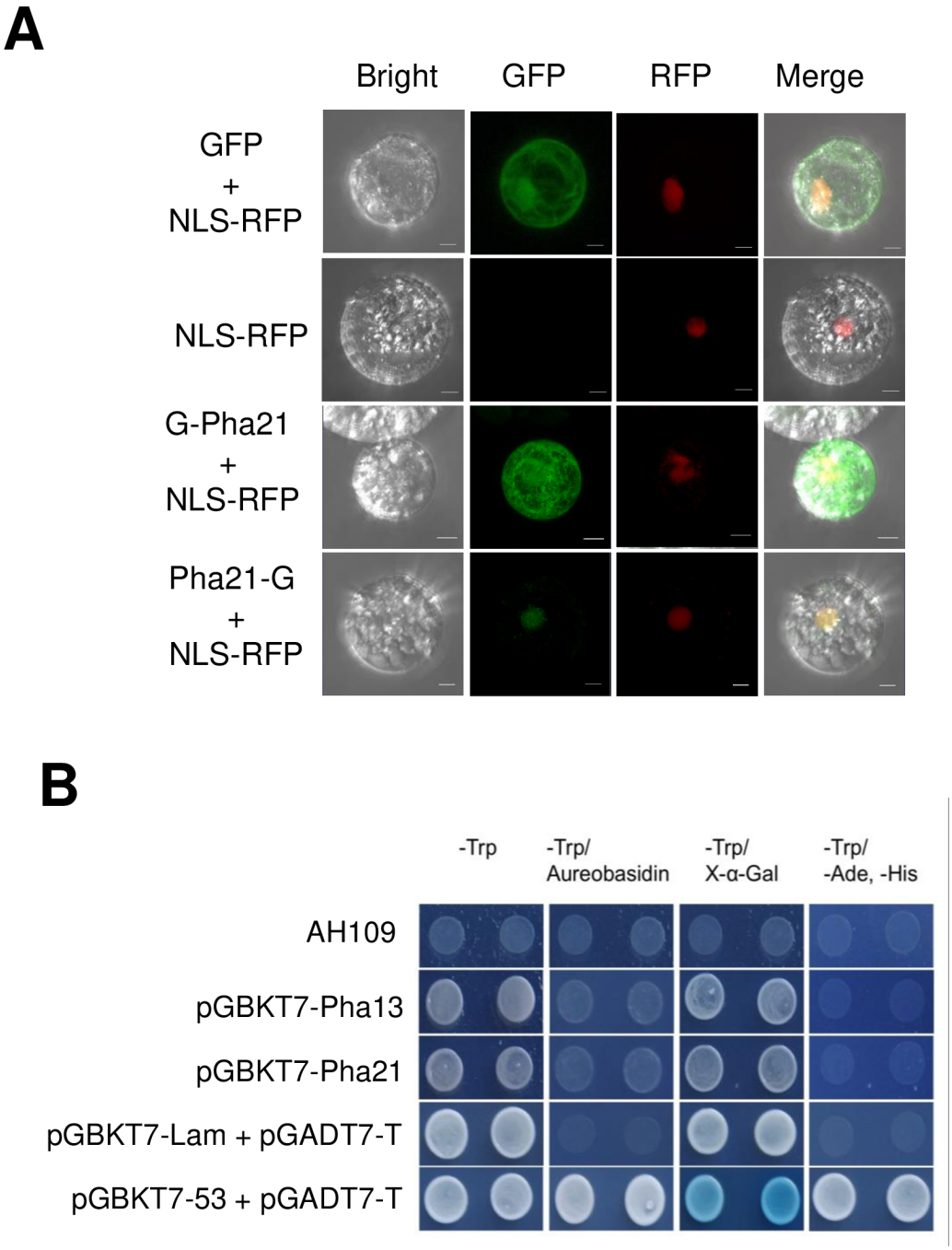

1049

1050

1051

1052

1053 **FIG 6**

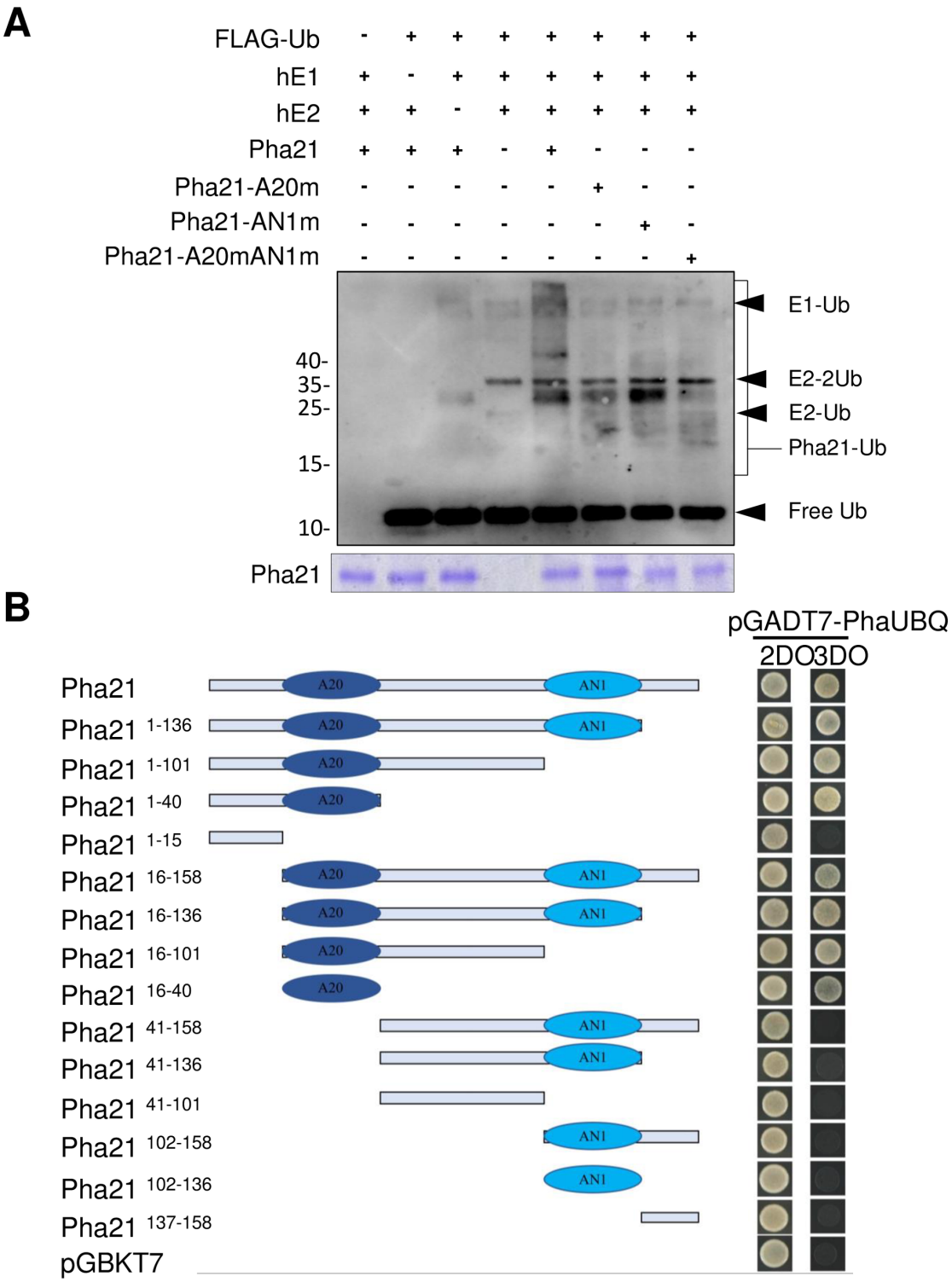

1054

1055

1056

1057 **FIG 7**

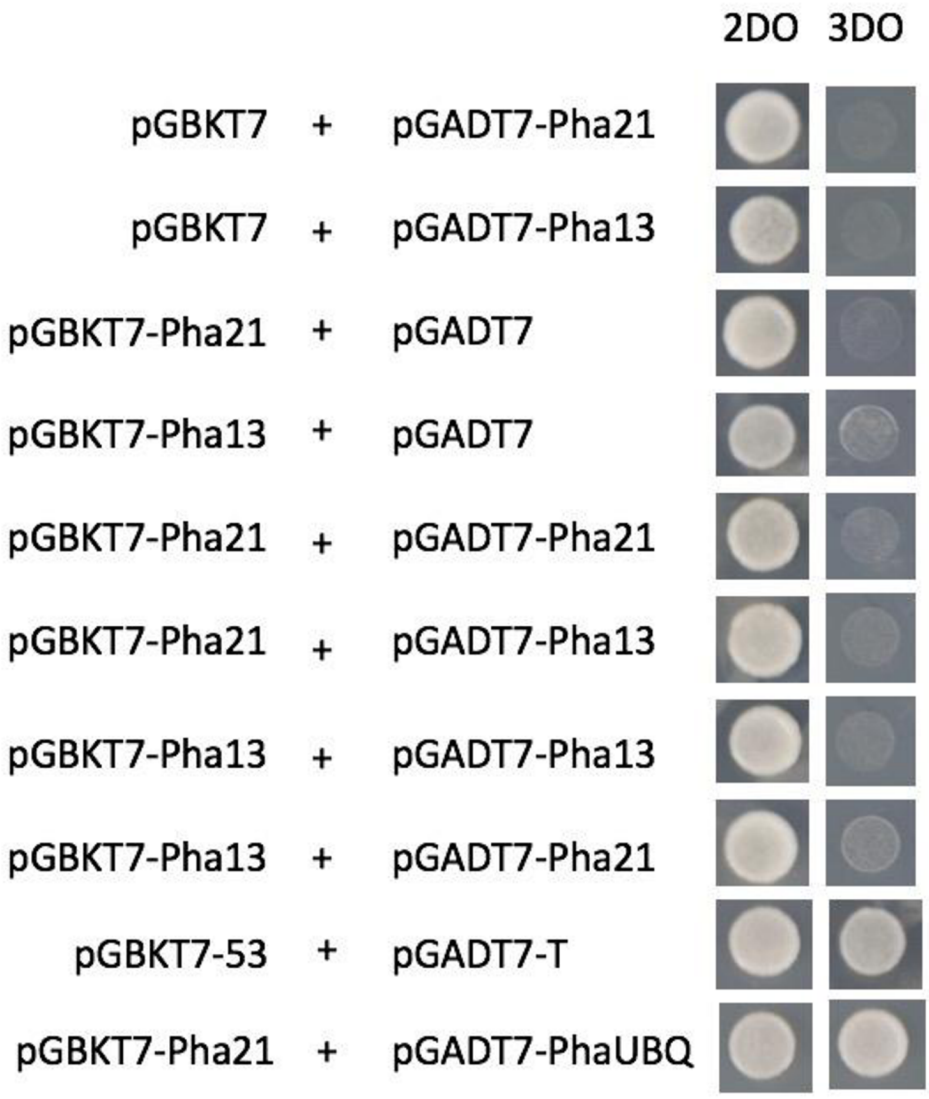

1072

1073

1074

1075

1076

1077

1078

1079 **FIG 8**

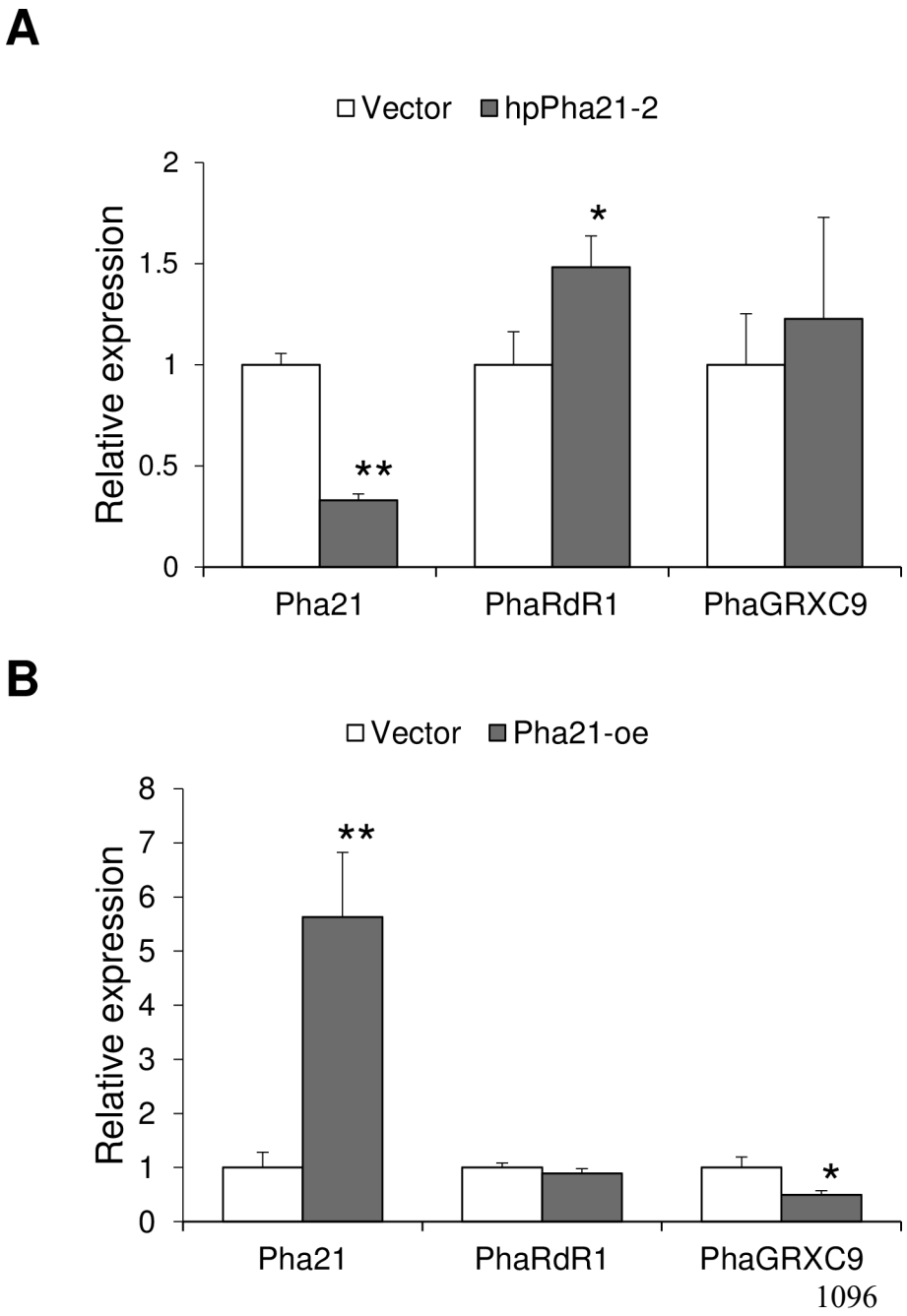

1096

1097

1098

1099

1100

1101 **FIG 9**

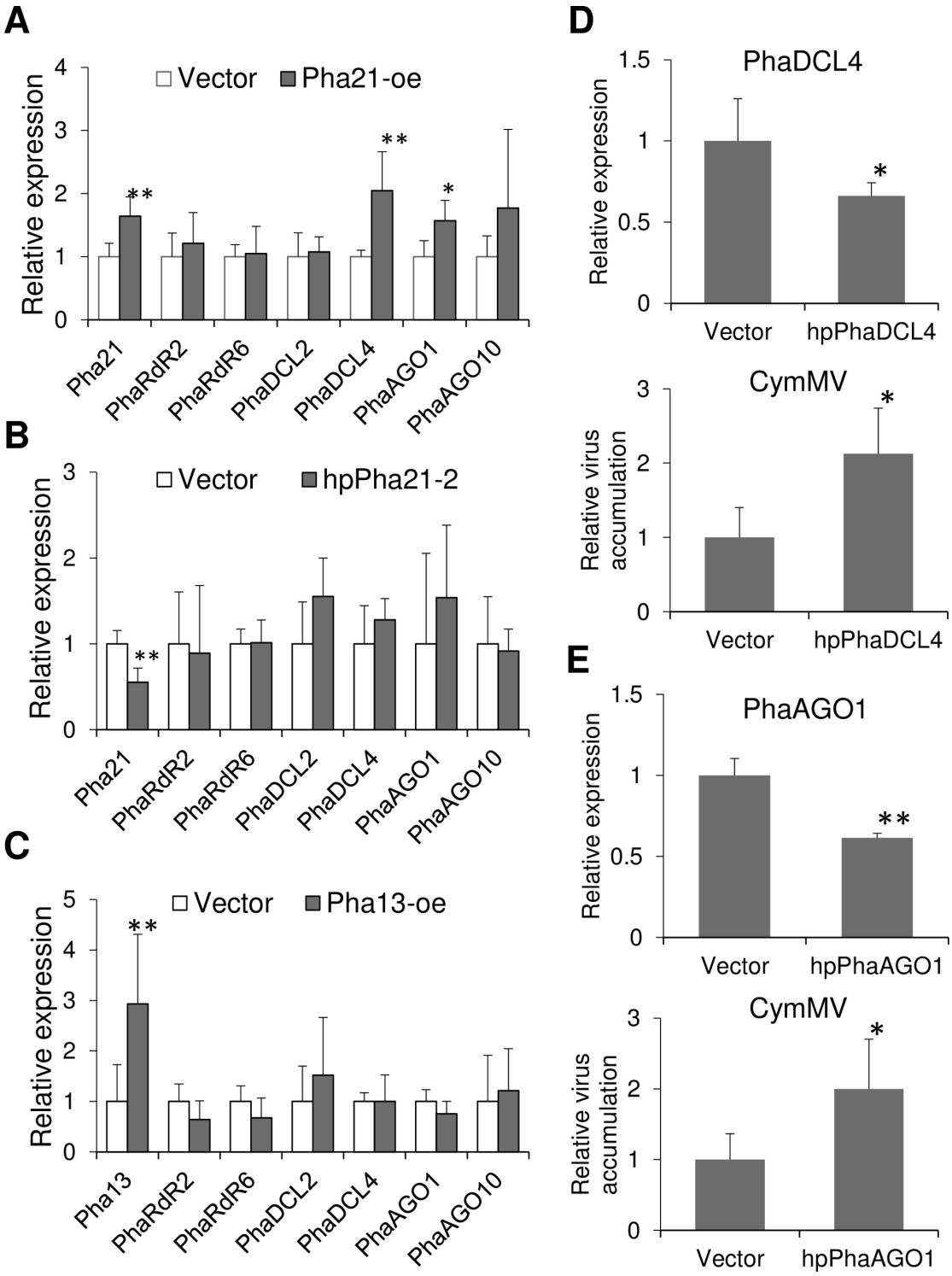

1102

1103

1104 **FIG 10**

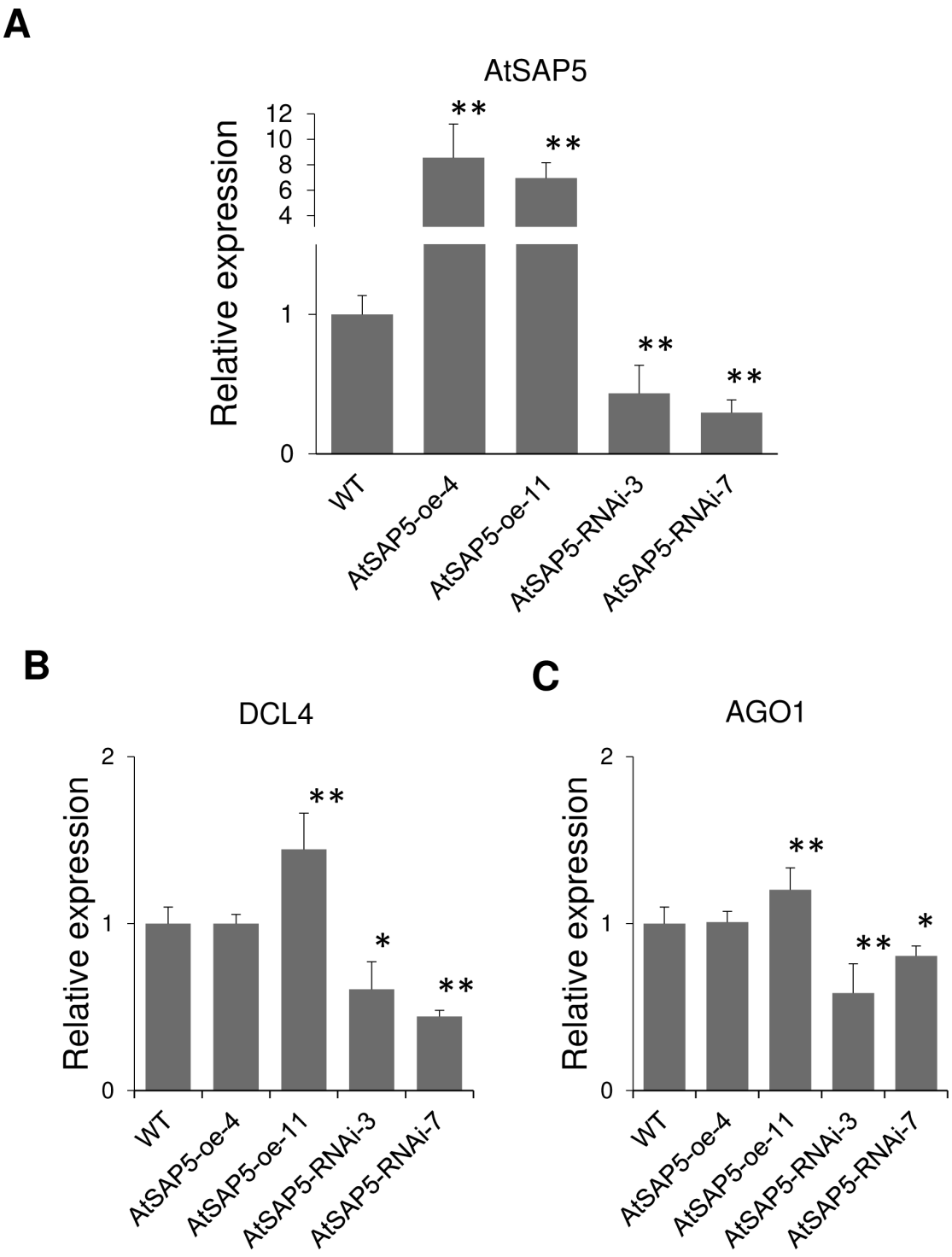

1105

1106

1107

1108 **FIG 11**

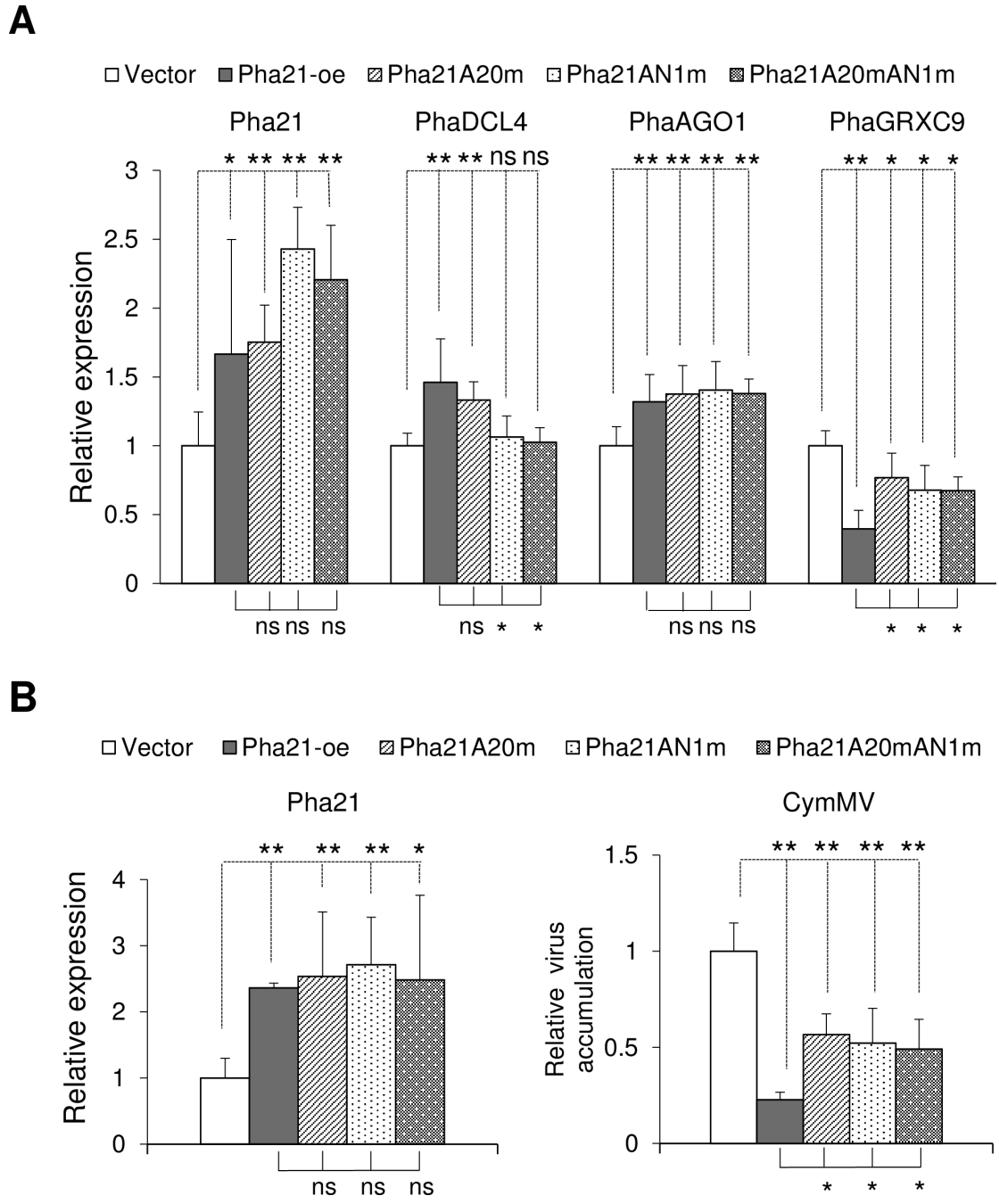

1109

1110

1111

1112 **FIG 12**

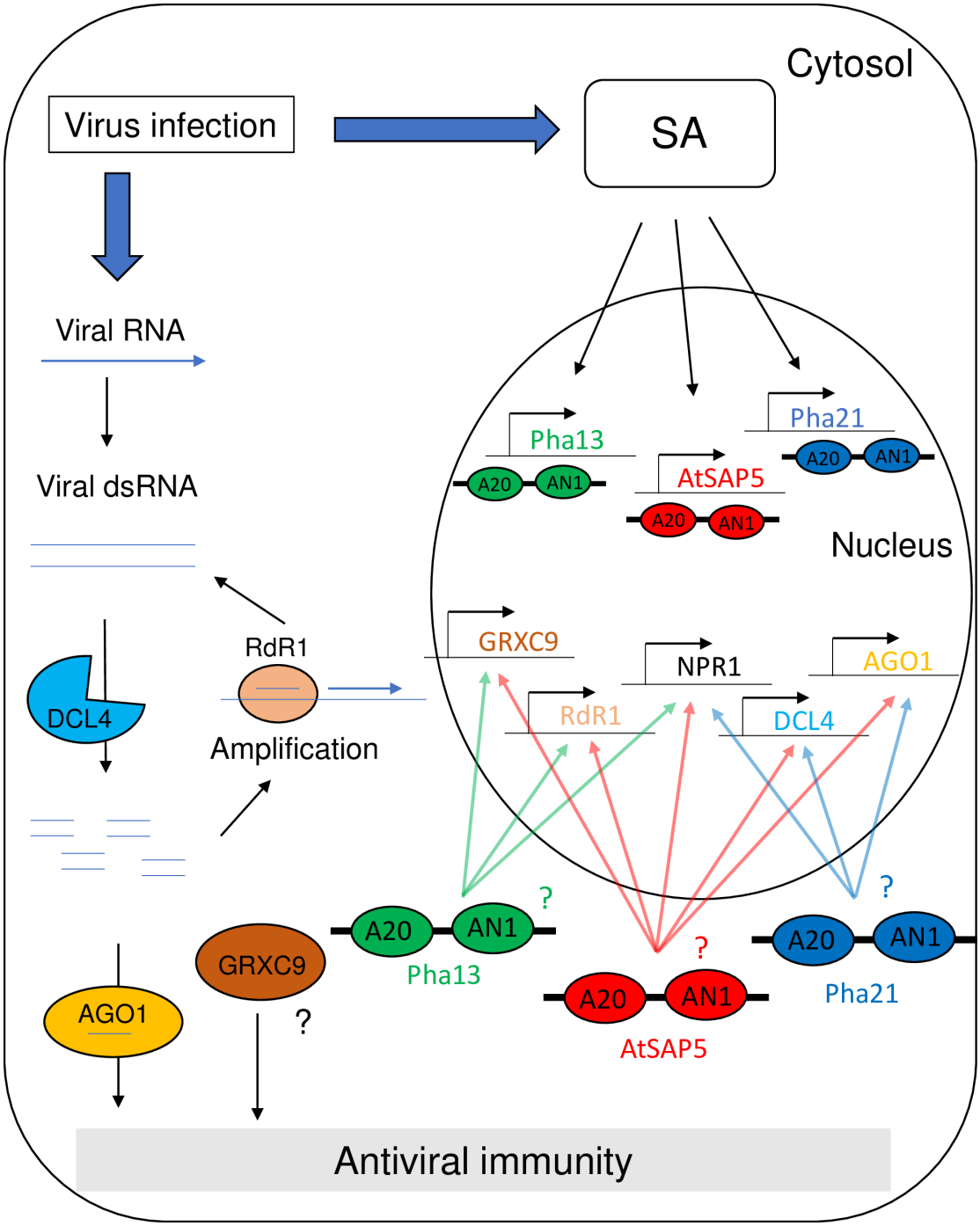

1113

1114

1115